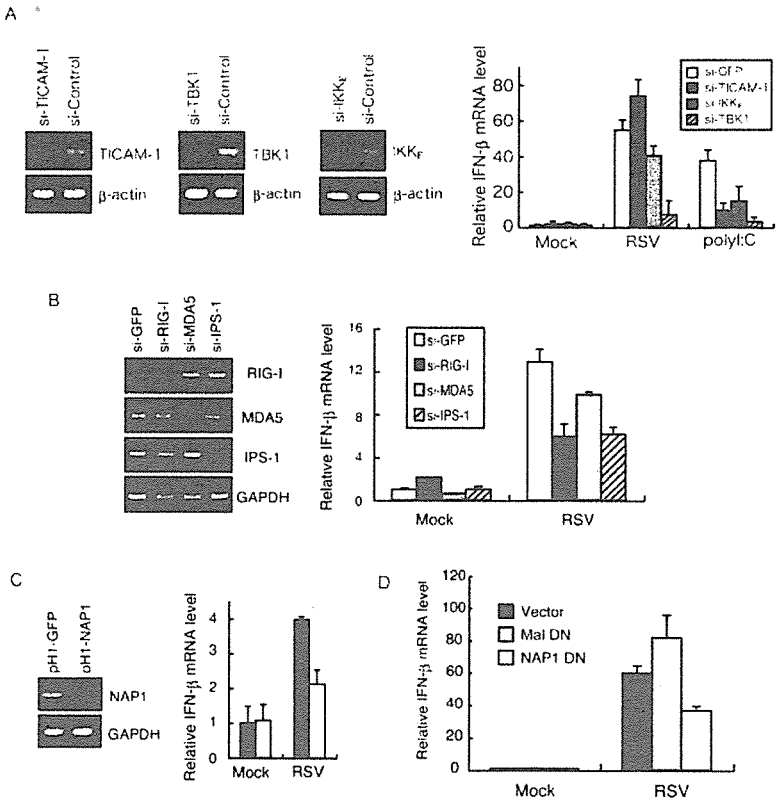

FIGURE 7. NAP1 is involved in IFN-β induction by RSV infection. *A*, HeLa cells were transfected with siRNA silencing for GFP, TICAM-1, IKKε, or TBK1. The indicated mRNAs levels shown after gene silencing were analyzed by RT-PCR. Cells were treated with RSV (MOI = 1 for 48 h) or poly(I:C) (10 μg/ml). Cells were lysed and mRNA levels of IFN-β were determined by Q-PCR. *B*, HeLa cells were transfected with siRNA silencing for GFP, RIG-I, MDA5, or IPS-1. The indicated mRNAs levels shown after gene silencing were analyzed by RT-PCR. Cells were treated with RSV (MOI = 2.5 for 48 h). *C*, HeLa stable clones of silencing NAP1 or GFP gene were infected with RSV (MOI = 1 for 48 h). The mRNAs levels of the cells are shown by RT-PCR. The mRNA levels of IFN-β were determined after RSV infection by Q-PCR. ■, GFP-silencing cells; □, NAP1-silencing cells. *D*, HEK293 cells were transiently transfected with the dominant-negative form of NAP1 or Mal/TIRAP. Twenty-four hours after transfection, cells were infected with RSV (MOI = 1 for 36 h). The mRNA levels of IFN-β in infected transfectants were measured as per *A*. Data are representative of two (*A–C*) or three (*D*) independent experiments.

the localization of NAP1 and IPS-1, Flag-tagged IPS-1 and *myc*-tagged NAP1 were expressed in HeLa cells, and merging analysis by confocal microscopy was performed. We confirmed that IPS-1 is the mitochondrial protein using our construct (data not shown). IPS-1 recruited NAP1 in the vicinity of the membrane (Fig. 3*C*). The results indicate that NAP1, at least in part, forms a complex with IPS-1 to relay the IRF-3-activating signal, although the reason why IPS-1 and NAP1 marginally coprecipitate with each other on immunoblotting remains unknown (Fig. 3*A*).

Concomitant functional analysis suggested that NAP1 DN blocks the IPS-1-mediated IFN-β promoter and IRF-3 activation (Fig. 4, *A* and *B*). Hence, there appear to be both physical and functional linkages between IPS-1 and NAP1. Thus, the results can be interpreted to most likely mean that the cytoplasmic (RIG-I/MDA5) and endosomal (TLR3) pathways converge on NAP1 to activate the IRF-3-activating kinases, leading to induction of IFN-β.

NAP1 DN and NAP1 decrease mediated inhibition of IFN induction by viral infection

Virus-mediated IRF-3 activation was examined with poly(I:C), VSV (Figs. 5 and 6), and RSV (Fig. 7), which are reported to activate cytoplasmic RIG-I and extracytoplasmic TLR3, respectively, to induce IFN promoter activation. Poly(I:C) is a reagent that activates the cytoplasmic IFN-inducing pathway in human cells in the presence of DEAE-dextran (Fig. 5*A*). HEK293 cells transfected with poly(I:C) using DEAE-dextran barely activated the IFN-β promoter in the reporter assay (*left-side* bars in Fig. 5*A*). When RIG-I and MDA5 were transfected into the cells before poly(I:C) stimulation, IFN-β promoter was activated by transfected poly(I:C), and NAP1-DN blocked those IFN-β promoter activation (Fig. 5*A*) and IRF-3 activation (data not shown). MDA5 prominently activated the IFN promoter compared with RIG-I, and this activity was efficiently impaired by co-transfection of NAP1 DN (Fig. 5*A*). Similar NAP1 DN-mediated suppression of IFN-β promoter activation was observed in cells without poly(I:C) (Fig. 5*A*), although the magnitude of the promoter activation was far less. A pervious study (29) demonstrated that VSV activates RIG-I in infected cells. VSV was subjected to the HEK293 cells instead of poly(I:C), and IRF-3 activation was tested in the reporter (data not shown) and native gel analyses (Fig. 5*B*). Under the conditions where IRF-3 is activated in response to VSV, NAP1 DN inhibited VSV-mediated IRF-3 activation in a dose-dependent manner (Fig. 5*B*). Thus, the results infer that RIG-I/MDA5 interacts with NAP1 in the virus-derived IFN-inducing pathway.

HeLa cell clones with stable gene silencing of NAP1 were established in an effort to confirm the essential role of NAP1 in virus-mediated IFN-β induction (Fig. 6*A*). IRF-3 dimer formation by VSV was apparently reduced in the NAP1-deficient cells (Fig. 6*B*). Concomitantly, the level of IFN-β mRNA was decreased in the NAP1-deficient cells (Fig. 6*C*). In this experiment, HeLa cell clones with the vector containing GFP siRNA were used as controls. Two NAP1-depleting clones of one target's site (site-A) and one depleting clone of another target site (site-B) showed similar low responses to VSV in IFN-β induction compared with the control (Fig. 6*C*), which excludes the possibility of artificial clonal effect. These results, together with the fact that VSV replication allows human cells to produce IFN-β in a RIG-I-dependent manner (29), suggest that NAP1 is indispensable to RIG-I-mediated IFN induction.

RSV is known to induce TLR3 responses in epithelial cells. RSV was used instead of VSV to confirm the effect on virus-activated IFN-β promoter activation in HeLa cells (Fig. 7). NAP1 as well as TICAM-1, IKKε, and TBK1 were silenced with siRNA, and the IFN-β mRNA levels were then measured in RSV-infected cells. Cells stimulated with poly(I:C) were used as control for the TICAM-1 pathway. As expected and consistent with previous reports, poly(I:C)-dependent IFN-β mRNA was found to be dependent on TICAM-1, IKKε, and TBK1 (Fig. 7*A*). Notably, TICAM-1 silencing had no

down-regulation effect on the IFN-β mRNA level, whereas IKKε and TBK1 were associated with RSV-mediated IFN induction (Fig. 7*A*). The IFN-β mRNA levels were evaluated 48 h after RSV infection in cells silencing of RIG-I, MDA5, or IPS-1. The IFN-β mRNA induction was most prominently impaired in cells depleted of RIG-I or IPS-1 (Fig. 7*B*). When NAP1 was silenced, 40% of the IFN-β mRNA level was reduced in the cells stimulated with poly(I:C) within 6 h (cells die during long-term incubation with poly(I:C)) (data not shown). In this system, RSV infection resulted in a 50% decrease of the NAP1-mediated IFN-β induction (Fig. 7*C*). To further confirm the involvement of NAP1 in the virus-mediated IFN-β-inducing pathway, we used the dominant-negative transfectants (Fig. 7*D*). No reduction of the IFN-β mRNA level was observed with the Mal/TIRAP dominant-negative-expressing HEK cells, whereas the IFN-β mRNA level was significantly decreased in cells expressing the NAP1 DN. Thus, RSV induces IFN-β independent of TICAM-1 but dependent on RIG-I, IPS-1, virus-activated kinases, and NAP1.

Discussion

In this study, we demonstrated that the CARD-helicase pattern-recognition receptors activate IRF-3 and the IFN promoter through NAP1, the regulatory subunit of the kinase complex IKKε and TBK1. The kinases IKKε and TBK1 are known to be virus-activated kinases (16) and are located downstream of TICAM-1 (also known as TRIF) (15). A previous study (18) revealed that NAP1 is also involved in a molecular complex containing TICAM-1. The N-terminal region out of the TIR domain of TICAM-1 participates in NAP1 recruitment. Thus, NAP1 works in the two different pathways for dsRNA-mediated IFN-β induction, TLR3/TLR4 followed by the TICAM-1 pathway and RIG-I/MDA5 followed by the IPS-1 pathway.

The results were consolidated with virus infection studies. RSV as well as VSV induces IFN-β in infected cells, and these viral IFN-inducing activities were blocked by NAP1 DN or siRNA, suggesting that NAP1 participates in virus-activated IRF-3 and IFN-β induction. NAP1 is implicated in the intracytoplasmic IFN-β-inducing signal in physical proximity to the molecular complex containing RIG-I and MDA5. Hence, NAP1 connects RNA sensor proteins (TLR3, RIG-I, and MDA5) and kinases to activate IRF-3. This scenario would be suitable to the findings of previous studies on IFN-β induction by cells with exogenously added poly(I:C) (18) and with replicated viruses (29).

NAP1 assembles IKKε and TBK1 to form a kinase complex (17). This kinase complex participates in activation of not only IRF-3 but also NF-κB. Actually, we have evidence that overexpression of RIG-I (particularly RIG-IN) or MDA5 in HEK cells results in activation of NF-κB and, under this situation, NAP1 DN blocks the NF-κB activation through RIG-I/MDA5 (data not shown). NF-κB activation through TNF-α receptors, however, revealed to involve two additional kinases, IKKα and IKKβ (30). Furthermore, two additional subunits, TANK and IKKγ, may affect the level of NF-κB activation (31). TLR4 as well as other TLRs principally activate NF-κB through IKKγ and a kinase complex with IKKα and IKKβ (32). In activation of NF-κB via NAP1, what combinations of the four kinases preferentially join the NAP1 protein complex still remains undetermined. Accordingly, molecular configuration of the kinase complex for activation of NF-κB remains to be defined downstream of IPS-1.

Using two species of viruses, VSV and RSV, RIG-I/MDA5 is evidently responsible for sensing viral infection to induce IFN-β. Previous reports have indicated that VSV stimulates the RIG-I pathway (33) and RSV induces TLR3 up-regulation and responses including cytokine/chemokine secretion in airway epithelial cells (4, 5, 20) Our gene silencing studies using siRNA (Fig. 7) and the RSV strain (an IFN-inducible strain) suggest that RIG-I is a key molecule in RSV-mediated IFN-β induction in HeLa cells. MDA5 or TLR3 minimally participates in RSV sensing, if any, in this in vitro study. VSV, a representative of the RIG-I-activating virus, confers a similar IFN-inducing profile to the RSV strain.

Hence, the involvement of TLR3 in the induction of type I IFN by RSV may reflect a secondary response resulting from TLR3 up-regulation by the initial production of IFN-β in virtue of RIG-I. We previously showed that NAP1 but not TANK interacts with TICAM-1 in the TLR3 pathway (18). Preferential recognition of RSV replication by RIG-I with no involvement of TLR3 and TICAM-1 appears to be additional evidence that NAP1 plays a major role downstream of RIG-I and outcome of viral infection. Because the results were obtained with HeLa and HEK293 cells in an acute-phase infection, this result should be confirmed with a cell line of bronchial epithelial cells and in vivo animal models.

However, it remains in question why IPS-1 only marginally coprecipitates with NAP1 in this study. According to the confocal analysis, NAP1 merges with IPS-1 on mitochondria. The discrepancy may be explained by the activation-induced mobility of IPS-1. IPS-1 overexpression leads to activation of the IFN-β promoter (Fig. 4*A*; Refs. 12, 13) and shows a merging profile with NAP1. A previous study (14) suggests that IPS-1 moves from a detergent-soluble to detergent-insoluble fraction in mitochondria following virus infection. The transposition of IPS-1 on the mitochondrial membrane may affect the dynamics of the cytoplasmic protein NAP1. So far, we have not yet established the system to see the molecular interaction between endogenous NAP1 and IPS-1. Maybe, the question lies in the artificial overexpression system. We favor the idea that IPS-1 forms a complex with NAP1, but the complex is fragile depending on the conditions where IPS-1 is disposed or solubilized from the mitochondrial membrane. Alternatively, NAP1 may only temporally bind IPS-1 on the mitochondrial membrane in initiating the pathway that activates IRF-3 in human cells. In this context, it is of interest to see the effect of viral infection on the molecular association between NAP1 and IPS-1.

Two further points remain to be discussed. First, our previous immunoprecipitation studies suggested that TICAM-1 forms a complex with NAP1 (18), whereas IPS-1 barely joins the complex containing TICAM-1 (data not shown). NAP1 coprecipitates with TICAM-1 irrespective of poly(I:C) activation of TLR3 (18). However, NAP1 does not merge with intrinsic TICAM-1 (data not shown), but with IPS-1 (Fig. 3*C*) largely around the mitochondria as shown by confocal analysis. The localization pattern of NAP1 is mysterious but may reflect the differential properties between TICAM-1 and IPS-1. Human cells mostly have a low level of TICAM-1 and a high level of IPS-1, and the level of TICAM-1 protein expression is usually suppressed because of its apoptosis-inducing properties (34). TICAM-1 undergoes protein modifications in response to poly(I:C) stimulation (M. Sasai and T. Seya, unpublished data), which may be a prerequisite for the recruitment of NAP1.

Secondly, RIG-I and MDA5 have been shown to be responsible for intracellular viral dsRNA recognition (33). They are cytoplasmic proteins of the CARD-helicase-containing family (22). RIG-I without a helicase domain (RIG-IN) acts as a constitutively active IFN inducer in transfected cells, whereas MDA5 expresses full IFN-inducing activity regardless of its helicase domain. The manner of ligand recognition may be somewhat different in each. Why RIG-I mainly participated in recognition of VSV/RSV infection is unknown. After completing this study, a report (29) was published showing that MDA5 preferentially recognizes poly(I:C) and the replicated RNAs of picornaviruses, whereas RIG-I recognizes transcribed dsRNAs of many RNA viruses. Although the report did not mention the natural ligand of MDA5, it offers evidence that MDA5 and RIG-I discriminate between the dsRNA structures

(29). Because RSV is a negative-strand RNA virus, it may hold a RNA structural motif inducing activation of RIG-I common to other negative-strand RNA viruses (35).

Pattern recognition molecules besides TLR3 and the CARD-helicase proteins are engaged in foreign RNA sensing in human cells. For example, TLR7 and TLR8 are expressed in human plasmacytoid DCs and mDCs, respectively (36). PKR is a receptor for dsRNA recognition (37). Generation of dsRNA may link to the pathway for inducing RNAi even in human cells. Why the host provides a variety of RNA pattern-recognition receptors and non-self RNA responses will be the issue to be clarified. Another point is that viral factors other than RNA have some host-immune-modulating functions. Measles nucleoproteins may modulate a Fcγ receptor-mediated immune response (38) and IRF-3 activation (39), which clearly occur independent of dsRNA or RNA replication. A recent report (40) suggests that negative-strand RNA viruses produce only undetectable amounts of dsRNA in infected cells. Although RIG-I is a key molecule in host protection against a number of RNA virus infections, other molecules and systems may be involved in host strategies against virus infection.

Acknowledgments

We are grateful to Drs. A. Ishii, T. Ebihara, and A. Matsuo in our laboratory for their critical discussions. Thanks are also due to Dr. K. Imai (Wakayama Prefectural Center, Wakayama, Japan) for providing us with RSV and to Drs. T. Fujita (Kyoto University, Kyoto, Japan), K. Miyake (Tokyo University, Tokyo, Japan), M. Nakanishi (the Nagoya City University, Nagoya, Japan), and T. Maniatis (Harvard Univeresity, Boston, MA) for providing their plasmids. Dr. Boru (Pacific Edit) reviewed this manuscript before submission.

Disclosures

The authors have no financial conflict of interest.

References

1. Akira, S., S. Uematsu, and O. Takeuchi. 2006. Pathogen recognition and innate immunity. *Cell* 124: 783–801.
2. Yoneyama, M., M. Kikuchi, T. Natsukawa, N. Shinobu, T. Imaizumi, M. Miyagishi, K. Taira, S. Akira, and T. Fujita. 2004. The RNA helicase RIG-I has an essential function in double-stranded RNA-induced innate antiviral responses. *Nat. Immunol.* 5: 730–737.
3. Matsumoto, M., K. Funami, M. Tanabe, H. Oshiumi, M. Shingai, Y. Seto, A. Yamamoto, and T. Seya. 2003. Subcellular localization of Toll-like receptor 3 in human dendritic cells. *J. Immunol.* 171: 3154–3162.
4. Rudd, B. D., J. J. Smit, R. A. Flavell, L. Alexopoulou, M. A. Schaller, A. Gruber, A. A. Berlin, and N. W. Lukacs. 2006. Deletion of TLR3 alters the pulmonary immune environment and mucus production during respiratory syncytial virus infection. *J. Immunol.* 176: 1937–1942.
5. Groskreutz, D. J., M. M. Monick, L. S. Powers, T. O. Yarovinsky, D. C. Look, and G. W. Hunninghake. 2006. Respiratory syncytial virus induces TLR3 protein and protein kinase R, leading to increased double-stranded RNA responsiveness in airway epithelial cells. *J. Immunol.* 176: 1733–1740.
6. Guillot, L., R. Le Goffic, S. Bloch, N. Escriou, S. Akira, M. Chignard, and M. Si-Tahar. 2005. Involvement of Toll-like receptor 3 in the immune response of lung epithelial cells to double-stranded RNA and influenza A virus. *J. Biol. Chem.* 280: 5571–5580.
7. Hall, C. B., K. R. Powell, N. E. MacDonald, C. L. Gala, M. E. Menegus, S. C. Suffin, and H. J. Cohen. 1986. Respiratory syncytial viral infection in children with compromised immune function. *N. Engl. J. Med.* 315: 77–81.
8. Yamamoto, M., S. Sato, H. Hemmi, K. Hoshino, T. Kaisho, H. Sanjo, O. Takeuchi, M. Sugiyama, M. Okabe, K. Takeda, and S. Akira. 2003. Role of adaptor TRIF in the MyD88-independent Toll-like receptor signaling pathway. *Science* 301: 640–643.
9. Oshiumi, H., M. Matsumoto, K. Funami, T. Akazawa, and T. Seya. 2003. TICAM-1, an adaptor molecule that participates in Toll-like receptor 3-mediated interferon-β induction. *Nat. Immunol.* 4: 161–167.
10. McWhirter, S. M., B. R. Tenoever, and T. Maniatis. 2005. Connecting mitochondria and innate immunity. *Cell* 122: 645–647.
11. Meylan, E., J. Curran, K. Hofmann, D. Moradpour, M. Binder, R. Bartenschlager, and J. Tschopp. 2005. Cardif is an adaptor protein in the RIG-I antiviral pathway and is targeted by hepatitis C virus. *Nature* 437: 1167–1172.
12. Kawai, T., K. Takahashi, S. Sato, C. Coban, H. Kumar, H. Kato, K. J. Ishii, O. Takeuchi, and S. Akira. 2005. IPS-1, an adaptor triggering RIG-I- and Mda5-mediated type I interferon induction. *Nat. Immunol.* 6: 981–988.
13. Xu, L. G., Y. Y. Wang, K. J. Han, L. Y. Li, Z. Zhai, and H. B. Shu. 2005. VISA is an adapter protein required for virus-triggered IFN-β signaling. *Mol. Cell* 19: 727–740.
14. Seth, R. B., L. Sun, C. K. Ea, and Z. J. Chen. 2005. Identification and characterization of MAVS, a mitochondrial antiviral signaling protein that activates NF-κB and IRF 3. *Cell* 122: 669–682.
15. Fitzgerald, K. A., S. M. McWhirter, K. L. Faia, D. C. Rowe, E. Latz, D. T. Golenbock, A. J. Coyle, S. M. Liao, and T. Maniatis. 2003. IKKϵ and TBK1 are essential components of the IRF3 signaling pathway. *Nat. Immunol.* 4: 491–496.
16. Sharma, S., B. R. tenOever, N. Grandvaux, G. P. Zhou, R. Lin, and J. Hiscott. 2003. Triggering the interferon antiviral response through an IKK-related pathway. *Science* 300: 1148–1151.
17. Fujita, F., Y. Taniguchi, T. Kato, Y. Narita, A. Furuya, T. Ogawa, H. Sakurai, T. Joh, M. Itoh, M. Delhase, et al. 2003. Identification of NAP1, a regulatory subunit of IκB kinase-related kinases that potentiates NF-κB signaling. *Mol. Cell. Biol.* 23: 7780–7793.
18. Sasai, M., H. Oshiumi, M. Matsumoto, N. Inoue, F. Fujita, M. Nakanishi, and T. Seya. 2005. Cutting Edge: NF-κB-activating kinase-associated protein 1 participates in TLR3/Toll-IL-1 homology domain-containing adapter molecule-1-mediated IFN regulatory factor 3 activation. *J. Immunol.* 174: 27–30.
19. Sasai, M., M. Matsumoto, and T. Seya. 2006. The kinase complex responsible for IRF-3-mediated IFN-β production in myeloid dendritic cells (mDC). *J. Biochem.* 139: 171–175.
20. Rudd, B. D., E. Burstein, C. S. Duckett, X. Li, and N. W. Lukacs. 2005. Differential role for TLR3 in respiratory syncytial virus-induced chemokine expression. *J. Virol.* 79: 3350–3357.
21. Yoneyama, M., W. Suhara, Y. Fukuhara, M. Fukuda, E. Nishida, and T. Fujita. 1998. Direct triggering of the type I interferon system by virus infection: activation of a transcription factor complex containing IRF-3 and CBP/p300. *EMBO J.* 17: 1087–1095.
22. Yoneyama, M., M. Kikuchi, K. Matsumoto, T. Imaizumi, M. Miyagishi, K. Taira, E. Foy, Y. M. Loo, M. Gale, Jr., S. Akira, et al. 2005. Shared and unique functions of the DExD/H-box helicases RIG-I, MDA5, and LGP2 in antiviral innate immunity. *J. Immunol.* 175: 2851–2858.
23. Oshiumi, H., M. Sasai, K. Shida, T. Fujita, M. Matsumoto, and T. Seya. 2003. TIR-containing adapter molecule (TICAM)-2, a bridging adapter recruiting to Toll-like receptor 4 TICAM-1 that induces interferon-β. *J. Biol. Chem.* 278: 49751–49762.
24. Iwamura, T., M. Yoneyama, K. Yamaguchi, W. Suhara, W. Mori, K. Shiota, Y. Okabe, H. Namiki, and T. Fujita. 2001. Induction of IRF-3/-7 kinase and NF-κB in response to double-stranded RNA and virus infection: common and unique pathways. *Genes Cells* 6: 375–388.
25. Funami, K., M. Matsumoto, H. Oshiumi, T. Akazawa, A. Yamamoto, and T. Seya. 2004. The cytoplasmic 'linker region' in Toll-like receptor 3 controls receptor localization and signaling. *Int. Immunol.* 16: 1143–1154.
26. Murabayashi, N., M. Kurita-Taniguchi, M. Ayata, M. Matsumoto, H. Ogura, and T. Seya. 2002. Susceptibility of human dendritic cells (DCs) to measles virus (MV) depends on their activation stages in conjunction with the level of CDw150: role of Toll stimulators in DC maturation and MV amplification. *Microbes Infect.* 4: 785–794.
27. Spielhofer, P., T. Bachi, T. Fehr, G. Christiansen, R. Cattaneo, K. Kaelin, M. A. Billeter, and H. Y. Naim. 1998. Chimeric measles viruses with a foreign envelope. *J. Virol.* 72: 2150–2159.
28. Hasuwa, H., K. Kaseda, T. Einarsdottir, and M. Okabe. 2002. Small interfering RNA and gene silencing in transgenic mice and rats. *FEBS Lett.* 532: 227–230.
29. Kato, H., O. Takeuchi, S. Sato, M. Yoneyama, M. Yamamoto, K. Matsui, S. Uematsu, A. Jung, T. Kawai, K. J. Ishii, et al. 2006. Differential roles of MDA5 and RIG-I helicases in the recognition of RNA viruses. *Nature* 441: 101–105.
30. Peters, R. T., and T. Maniatis. 2001. A new family of IKK-related kinases may function as IκB kinase kinases. *Biochim. Biophys. Acta* 1471: M57–M62.
31. Rothe, M., J. Xiong, H. B. Shu, K. Williamson, A. Goddard, and D. V. Goeddel. 1996. I-TRAF is a novel TRAF-interacting protein that regulates TRAF-mediated signal transduction. *Proc. Natl. Acad. Sci. USA* 93: 8241–8246.
32. Akira, S., K. Takeda, and T. Kaisho. 2001. Toll-like receptors: critical proteins linking innate and acquired immunity. *Nat. Immunol.* 2: 675–680.
33. Kawai, T., and S. Akira. 2006. Innate immune recognition of viral infection. *Nat. Immunol.* 7: 131–137.
34. Han, K. J., X. Su, L. G. Xu, L. H. Bin, J. Zhang, and H. B. Shu. 2004. Mechanisms of TRIF-induced ISRE and NF-κB activation and apoptosis pathways. *J. Biol. Chem.* 279: 15652–15661.
35. Melchjorsen, J., S. B. Jensen, L. Malmgaard, S. B. Rasmussen, F. Weber, A. G. Bowie, S. Matikainen, and S. R. Paludan. 2005. Activation of innate defense against a paramyxovirus is mediated by RIG-I and TLR7 and TLR8 in a cell-type-specific manner. *J. Virol.* 79: 12944–12951.
36. Iwasaki, A., and R. Medzhitov. 2004. Toll-like receptor control of the adaptive immune responses. *Nat. Immunol.* 5: 987–995.
37. Mogensen, T. H., and S. R. Paludan. 2005. Reading the viral signature by Toll-like receptors and other pattern recognition receptors. *J. Mol. Med.* 83: 180–192.
38. Marie, J. C., F. Saltel, J. M. Escola, P. Jurdic, T. F. Wild, and B. Horvat. 2004. Cell surface delivery of the measles virus nucleoprotein: a viral strategy to induce immunosuppression. *J. Virol.* 78: 11952–11961.
39. tenOever, B. R., M. J. Servant, N. Grandvaux, R. Lin, and J. Hiscott. 2002. Recognition of the measles virus nucleocapsid as a mechanism of IRF-3 activation. *J. Virol.* 76: 3659–3669.
40. Weber, F., V. Wagner, S. B. Rasmussen, R. Hartmann, and S. R. Paludan. 2006. Double-stranded RNA is produced by positive-strand RNA viruses and DNA viruses but not in detectable amounts by negative-strand RNA viruses. *J. Virol.* 80: 5059–5064.

Intelectin: A Novel Lipid Raft-Associated Protein in the Enterocyte Brush Border†

Uta Wrackmeyer,‡ Gert H. Hansen,‡ Tsukasa Seya,§ and E. Michael Danielsen*,‡

Department of Medical Biochemistry and Genetics, Panum Institute, University of Copenhagen, Blegdamsvej 3, DK-2200 Copenhagen N, Denmark, and Department of Microbiology and Immunology, Hokkaido University Graduate School of Medicine, Kita-ku, Kita-15, Nishi-7, Sapporo 060-8638, Japan

Received March 22, 2006; Revised Manuscript Received June 1, 2006

ABSTRACT: Intelectin is a mammalian Ca^{2+}-dependent, D-galactosyl-specific lectin expressed in Paneth and goblet cells of the small intestine and proposed to serve a protective role in the innate immune response to parasite infection. In addition, it is structurally identical to the intestinal lactoferrin receptor known to reside in the enterocyte brush border. To clarify this apparent discrepancy with regard to localization, the aim of this work was to study the cellular and subcellular distribution of small intestinal intelectin by immunofluorescence and immunogold electron microscopy. Secretory granules of lysozyme-positive Paneth cells in the bottom of the crypts as well as goblet cells along the crypt−villus axis were intensively labeled with intelectin antibodies, but quantitatively, the major site of intelectin deposition was the enterocyte brush border. This membrane is organized in stable glycolipid-based lipid raft microdomains, and like the divalent lectin galectin-4, intelectin was enriched in microvillar "superrafts", i.e., membranes that resist solubilization with Triton X-100 at 37 °C. This strategic localization suggests that the trimeric intelectin, like galectin-4, serves as an organizer and stabilizer of the brush border membrane, preventing loss of digestive enzymes to the gut lumen and protecting the glycolipid microdomains from pathogens.

The small intestinal brush border is specifically designed to act both as a high-throughput digestive/absorptive surface and as a permeability barrier preventing lumenal pathogens from gaining access to the organism (*1*, *2*). To accomplish these tasks, the microvillar membrane is organized into stable lipid raft microdomains, mainly by virtue of its high content of glycolipids (*3*, *4*) and galectin-4, a divalent β-galactoside-recognizing lectin able to cross-link glycoconjugates (*5*, *6*). The extraordinary stability of these microdomains has been documented by their resistance to extraction with the detergent Triton X-100 at 37 °C, which induces them to form "superraft" membranes (*7*). Together, these superraft components are able to cluster many of the microvillar digestive hydrolases and thereby minimize their loss to the gut lumen due to proteolytic and lipolytic activities and exposure to bile salts (*8*). Unfortunately, the high-density glycolipid-based microdomains may also serve as portals for a large number of pathogens that specifically recognize glycolipids in their initial contact with a target epithelial cell (*9*−*13*). As the first line of defense against such pathogens, the invaded organism relies on secretion of antibodies (*14*), and "anti-glycosyl" antibodies, i.e., antibodies induced in the host by a glycosyl antigen (*15*), were recently shown to be deposited in the intestinal brush border (*16*). These lectin-like antibodies were thought to offer mucosal protection by competing with pathogens for binding sites at the brush border having terminal galactosyl residues.

In addition to galectin-4 and anti-glycosyl antibodies, other carbohydrate-recognizing proteins may well participate in mucosal brush border protection and pathogen surveillance. Thus, intelectin is a lectin expressed in the digestive tract. Its cloning and sequencing from the mouse revealed it to be homologous to *Xenopus laevis* lectin XL35, a Ca^{2+}-dependent, D-galactosyl-specific lectin (*17*, *18*). By in situ hybridization, intelectin expression was demonstrated specifically in Paneth cells of the small intestinal crypts (*19*). More recently, human intelectin was cloned and shown to have a high level of homology with the mouse protein (*20*). Human intelectin was affinity purified by chromatography on galactose-Sepharose, and its lectin properties also revealed an affinity for D-pentoses and a D-galactofuranosyl residue in the presence of Ca^{2+}. Intelectin has since been shown to exist in two isoforms in the small intestine, intelectin-1 and -2, whose amino acid sequences are 91% identical (*21*, *22*). Interestingly, intelectin-2 is expressed in goblet cells and is induced by infection with the nematode *Trichinella spiralis*, suggesting a protective role for this isoform in the innate immune response to parasite infection (*22*, *23*).

The enterocyte brush border membrane has long been known to harbor a receptor for lactoferrin, the member of the transferrin family of iron-binding proteins principally found in milk (*24*). Interestingly, the cloning and sequencing of the human small intestinal lactoferrin receptor (LfR)[1] have revealed its total identity with human intelectin (*20*, *25*).

† This work was supported by grants from the Danish Medical Research Council, the Novo-Nordic Foundation, the Beckett Foundation, and the Augustinus Foundation.

* To whom correspondence should be addressed: Department of Medical Biochemistry and Genetics, Building 6.4, Panum Institute, Blegdamsvej 3, DK-2200 Copenhagen N, Denmark. Phone: +4535327786. Fax: +4535367980. E-mail: midan@imbg.ku.dk.

‡ University of Copenhagen.

§ Hokkaido University Graduate School of Medicine.

[1] Abbreviations: DRM, detergent-resistant membrane; GPI, glycosylphosphatidylinositol; LfR, lactoferrin receptor; SDS−PAGE, sodium dodecyl sulfate−polyacrylamide gel electrophoresis.

10.1021/bi060570x CCC: $33.50
Published on Web 07/06/2006

Whereas some of the non-immune, antimicrobial functions ascribed independently to intelectin and LfR can easily be reconciled, the available data concerning the precise mucosal localization (enterocytes vs Paneth and goblet cells) of the two proteins are conflicting. This work was therefore undertaken to study in greater detail the cellular and subcellular distribution of intelectin in the small intestine. By immunofluorescence and immunogold electron microscopy, intelectin was localized both to Paneth cells in the bottom of the crypts and to goblet cells along the entire crypt−villus axis. Quantitatively, however, the brush border of the epithelium was the predominant site of intelectin deposition in the small intestine. Furthermore, intelectin was found to be a major component of microvillar lipid rafts and superrafts. This observation thus highlights the strategic importance of these glycolipid-rich microdomains in the mucosal defense against microorganisms.

MATERIALS AND METHODS

Materials. The rabbit antibodies to human intelectin (hIntL) were described previously (*20*). Briefly, rabbits were immunized with hIntL-transfected RK-13 cells with complete Freund's adjuvant. Immunoglobulins were isolated from the antiserum by ammonium sulfate fractionation, and the hIntL-specific antibodies were purified by affinity chromatography on recombinant hIntL bound to Affi-Gel 10 (Bio-Rad). Sheep antibodies to lysozyme were obtained from Abcam (Cambridge, U.K.), goat antibodies to annexin A2 from Santa Cruz (Santa Cruz, CA), rabbit antibodies to alkaline phosphatase from Biogenesis (Poole, U.K.), and rabbit antibodies to human lactoferrin and secondary antibodies for immunogold labeling from Dako Cytomation (Glostrup, Denmark). Secondary Alexa 488/594-conjugated antibodies were from Molecular Probes (Eugene, OR), and human lactoferrin and FITC-conjugated antibodies to human lactoferrin were from ICN (Costa Mesa, CA).

Pig and mouse small intestines were kindly provided by the Department of Experimental Medicine, Panum Institute, Copenhagen, Denmark. Paraffin-embedded pig kidney cortex was kindly given by C. Ørskov (Department of Medical Anatomy, Panum Institute).

Lactoferrin Binding and Uptake Studies in Organ-Cultured Mucosal Explant. The small intestines of adult mice, fasted overnight, were rinsed in MEM medium, and mucosal explants were excised and cultured in MEM medium essentially as described previously (26). The explants were cultured for 30 min at 4 or 37 °C in the presence of lactoferrin (0.5 mg/mL) in MEM medium, adjusted to pH 6.5. Control explants were cultured in the absence of lactoferrin in parallel.

Fluorescence Microscopy. The mucosal explants were fixed in 4% paraformaldehyde in 0.1 M sodium phosphate buffer (pH 7.2) (PB) for 2 h at 4 °C. After being rinsed in PB, the explants were frozen in precooled 2-methylbutane and mounted on a precooled cryostat table. Sections were cut in a Leitz cryostat at −20 °C, collected on glass slides, and incubated with a FITC-conjugated antibody to human lactoferrin.

In other experiments, sections of small intestine and kidney cortex were fixed as described above and embedded in paraffin. Rehydrated paraffin sections were incubated with primary antibodies (anti-intelectin, anti-lysozyme, and anti-aminopeptidase N), followed by fluorescent secondary antibodies. Control experiments with omission of primary antibodies were routinely performed in parallel. After being labeled, the sections were mounted in antifade mounting medium (DAKO, Glostrup, Denmark) and finally examined with a Leica DM 4000 B microscope equipped with a Leica DC 300 FX camera.

Immunogold Electron Microscopy. For Epon sectioning, pieces of pig small intestines were fixed in a 3% glutaraldehyde/2% paraformaldehyde mixture in PB for 30 min at 4 °C and membrane pellets of microvillar vesicles and superrafts in 2.5% glutaraldehyde in PB for 2 h at 4 °C.

After being rinsed in PB, the sections were postfixed in 1% osmium tetroxide in PB for 1 h at 4 °C, dehydrated in acetone, and finally embedded in Epon. Ultrathin sections were cut in an LKB Ultrotome III ultramicrotome, and the sections were incubated with anti-intelectin antibodies followed by labeling with 13 nm gold particles, prepared according to the method of Slot and Geuze (*27*) and conjugated to anti-rabbit immunoglobulins, as previously described (*28*). Control experiments with omission of the primary antibodies were performed in parallel. The sections were stained in 1% uranyl acetate in H_2O and lead citrate.

For ultracryosectioning, pieces of pig small intestine were fixed in a 2% paraformaldehyde/0.1% glutaraldehyde mixture in PB for 2 h at 4 °C, and mouse small intestinal mucosal explants cultured for 30 min at 4 or 37 °C in the presence of lactoferrin were fixed in 4% paraformaldehyde in PB for 2 h at 4 °C. After being rinsed in PB, the tissues were immersed in 2.3 M sucrose overnight, mounted on top of a metal pin, and frozen in liquid nitrogen. Ultracryosections were cut in a RMC MT 6000-XL ultracryomicrotome, collected using a sucrose droplet, and attached to Formvar-coated nickel grids. Immunogold labeling was performed using antibodies against intelectin and lactoferrin as previously described (*29*).

Finally, the Epon and ultracryosections were examined with a Zeiss EM 900 electron microscope equipped with a Mega View camera system.

Subcellular Fractionation. Microvillar vesicles were prepared from mouse and pig small intestine by the divalent cation precipitation method (*30*). Briefly, mucosal scrapings were homogenized in 2 mM Tris-HCl and 50 mM mannitol (pH 7.1) containing 10 μg/mL aprotinin and leupeptin by using a manually operated Potter-Elvehjem homogenizer. The homogenate was cleared by centrifugation at 500*g* for 10 min, and $MgCl_2$ was added to a final concentration of 10 mM. After 15 min on ice, the preparation was centrifuged at 1500*g* for 10 min to pellet intracellular and basolateral membranes. The supernatant was collected and centrifuged at 48000*g* for 1 h to obtain a pellet of microvillar membrane vesicles and a supernatant of soluble proteins.

For preparation of lipid rafts ("DRMs"), microvillar membranes were resuspended in 1 mL of HEPES-HCl and 150 mM NaCl (pH 7.1) containing 10 μg/mL aprotinin and leupeptin and extracted with 1% Triton X-100 for 10 min on ice. DRMs were isolated by sucrose gradient ultracentrifugation as described previously (*31*) with the modification that the extract was placed in a 60% sucrose cushion with a 50 to 25% sucrose gradient layered on top. The extract was centrifuged in an SW40 Ti rotor (Beckman Instruments, Palo

Alto, CA) for 20−22 h at 35 000 rpm (g_{max} = 217 000), as described previously (*32*). After centrifugation, the floating DRMs were carefully collected with a pipet, diluted five times with 25 mM HEPES-HCl and 150 mM NaCl (pH 7.1), and centrifuged at 48000*g* for 1 h to obtain a pellet of DRMs. For preparation of superrafts, DRMs were subsequently resuspended in 25 mM HEPES-HCl and 150 mM NaCl (pH 7.1) and extracted with 1% Triton X-100 for 10 min at room temperature, followed by reextraction at 37 °C, as previously described (*7*).

SDS−PAGE and Immunoblotting. SDS−PAGE in 15% gels was performed as described previously (*33*). After electrophoresis and electrotransfer of proteins onto Immobilon PVDF membranes, immunoblotting was performed with antibodies to alkaline phosphatase and annexin A2. The blots were developed with an electrochemiluminescence detection reagent kit according to the protocol supplied by the manufacturer (Amersham Biosciences, Little Chalfont, U.K.). After immunoblotting, total protein was visualized by staining with Coomassie brilliant blue R250 [0.2% dissolved in a methanol/H_2O/acetic acid mixture (50:43:7) for 1 min], followed by destaining in the same solvent for 30 min.

MALDI-TOF Analysis. Superraft membranes, prepared from mouse microvillar membrane vesicles, were subjected to SDS−PAGE in a 15% gel and electrotransferred onto an Immobilon PVDF membrane. After protein staining, a 35−40 kDa band was carefully excised and submitted to commercial MALDI-TOF analysis (Alphalyse, Odense, Denmark). Six peptides were identified, matching the amino acid sequences of residues 51−59, 156−163, 190−198, 230−239, 302−313, and 303−313 of intelectin (molecular mass of 34 995 Da) of *Mus musculus*. In addition, two bands of ~15−20 kDa were excised that generated peptides matching eight and 10 amino acid sequences, respectively, of galectin-4 (molecular mass of 36 602 Da) of *M. musculus*.

RESULTS

Immunofluorescence Localization of Intelectin. The intelectin gene was originally cloned from mice where it was shown by in situ hybridization to be expressed in intestinal Paneth cells (*19*), and it was proposed to function as a lectin because the deduced amino acid sequence revealed a level of homology with a *Xenopus laevis* oocyte lectin of 61% (*34*).

Figure 1A shows an immunofluorescence localization of intelectin along the crypt−villus axis of pig small intestine, using an immunopurified rabbit anti-human intelectin antibody previously described (*20*). The entire enterocyte brush border surface of the epithelium was distinctly labeled. In addition, an intense intracellular labeling was seen in goblet cells both in villi and in crypts. At higher magnifications, a faint labeling was also seen along the basolateral sides of the enterocytes as well as in a subapical region of the cells. For goblet cells, the intense labeling was confined to the apical pole of the cells (Figure 1B,C).

Paneth cell expression of intelectin was studied by double immunofluorescence labeling with the Paneth cell marker lysozyme (*35−37*). Along the epithelium, antibodies to lysozyme labeled only very few cells located near the bottom of the crypts (Figure 2A), but in addition, positive staining

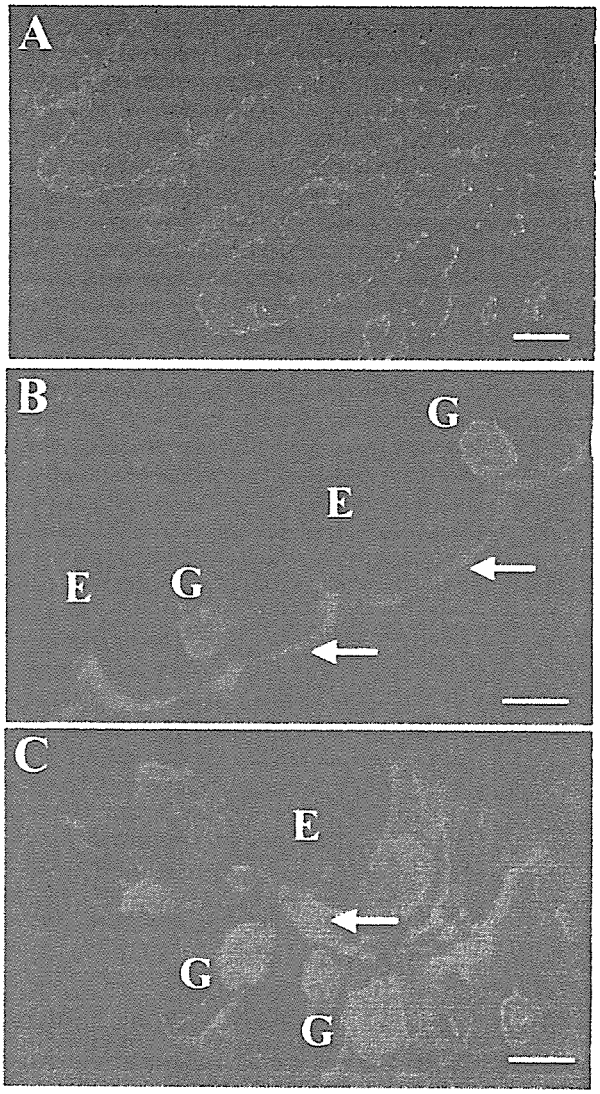

FIGURE 1: Localization of intelectin in the small intestine by immunofluorescence microscopy. (A) Longitudinal section of pig small intestinal mucosa labeled with anti-intelectin. A distinct staining of the brush border surface is seen along villi and crypts. In addition, goblet cells appear as strongly labeled dots along the entire crypt−villus axis. No labeling is present in the lamina propria region of the mucosa. (B and C) Higher-magnification images of the villus and crypt regions, respectively, showing labeling of goblet cells (G), enterocytes (E), and the brush border (arrows). Bars are 100 (A) and 10 μm (B and C).

was also found in a few cells of the lamina propria, as previously reported by others (data not shown) (*35*). As shown (Figure 2B,C), Paneth cells were clearly among the intelectin-positive cells located in the crypts, although they were clearly outnumbered by neighboring goblet cells.

Altogether, these results indicate that not only Paneth cells but also goblet cells, and possibly enterocytes, express intelectin. The complete absence of labeling of the lamina propria and the submucosa is indicative of the specificity of the antibody that was used. The antibody gave only a faint labeling of mouse intestinal epithelial cells (data not shown).

Intelectin expression was also studied by immunofluorescence microscopy in sections of kidney cortex. The kidney

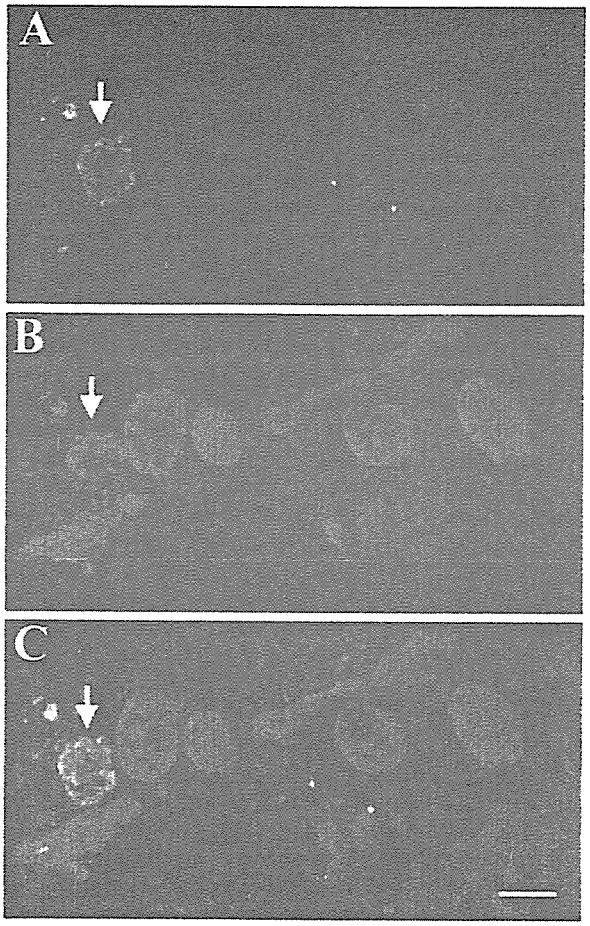

FIGURE 2: Double immunofluorescence labeling of lysozyme and intelectin. Crypt region labeled for lysozyme (A) and intelectin (B). Only one cell (arrow) in the section is lysozyme-positive, identifying it as a Paneth cell, whereas several cells as well as the luminal brush border are intelectin-positive. The merged image (C) shows that the Paneth cell is also labeled with the intelectin antibody. The bar is 10 μm.

proximal tubule cell resembles the enterocyte morphologically and expresses many of the intestinal brush border enzymes, including aminopeptidase N, and intelectin expression was likewise observed apically in this cell type (Figure 3). A similar labeling pattern for intelectin/LfR was previously demonstrated in mouse kidney by immunohistochemistry (*42*), and since gobletlike cells are not present in the kidney proximal tubule epithelium, this indicates that the proximal tubule cell itself synthesizes the protein.

Immunogold Localization of Intelectin in Enterocytes and Goblet Cells. A high-resolution subcellular localization of intelectin in the small intestine was performed by immunogold electron microscopy. Intense labeling was observed over the secretory granules, but endoplasmic reticulum membranes adjacent to the granular regions were also labeled (Figure 4A). Figure 4B shows the intense labeling of the secretory granules clustered in the apical pole of a goblet cell. The gold particles were evenly distributed inside the lumen of the granules, indicating that goblet cells express and secrete a soluble form of intelectin. A micrograph of the same cell taken at a higher magnification revealed an ongoing degranulation with microvilli from neighboring

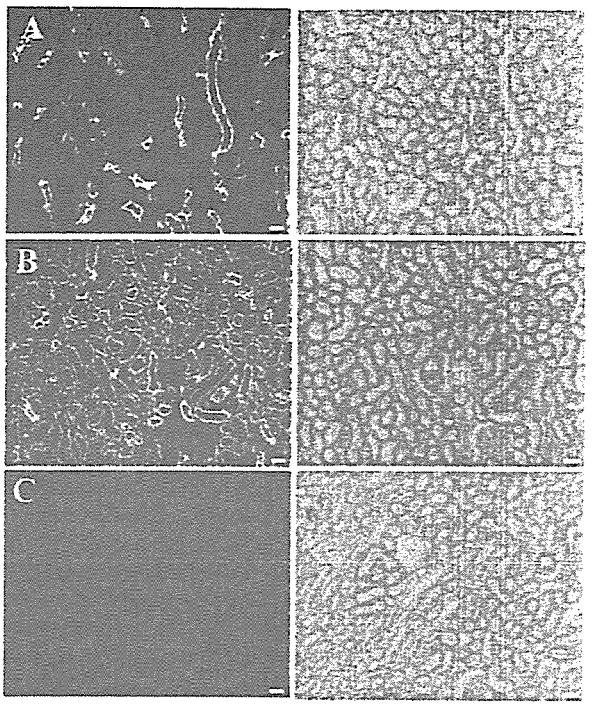

FIGURE 3: Localization of intelectin in the kidney. Paraffin-embedded sections of pig kidney cortex labeled for intelectin (A) and aminopeptidase N (B). For both proteins, the labeling was confined to the apical region of the proximal tubule cells, but unlike aminopeptidase N, intelectin was expressed in only a subset of the tubules. No labeling was detected when the primary antibody was omitted (C). The panels to the right show the corresponding sections recorded by incident light microscopy. The bar is 50 μm.

enterocytes in the proximity becoming decorated with intelectin in the process (Figure 4C).

The brush border membrane of enterocytes in both the crypt and villus region was also labeled with the anti-intelectin antibody (Figure 5), and a considerable variation in labeling intensity between neighboring enterocytes was occasionally observed (Figure 5A). Generally, labeling was seen along the entire length of the microvilli, and frequently, large aggregates of gold particles localized to invaginations between microvilli and to vesicle-like structures just below the apical surface (Figure 5B). Aggregates of gold particles were also present in multivesicular bodies in the subapical region, implying an ongoing internalization of intelectin (Figure 5C). A much weaker labeling was observed in the Golgi complex deeper in the cytoplasm of enterocytes (Figure 5D). No large aggregates of gold particles were observed in this compartment, and the labeling was confined to the membranes rather than to the lumen of the Golgi cisternae. Finally, a relatively faint labeling was observed along the basolateral surface of the enterocytes (data not shown).

In conclusion, the immunogold localization of intelectin confirmed its presence in both goblet cells and enterocytes. Although the granules of the goblet cells were by far the most intensely labeled structures, the enterocyte brush border membrane is a major site of intelectin deposition in the intestinal epithelium. The brush border intelectin most likely originates mainly from neighboring degranulating goblet cells. However, the faint but distinct labeling of the Golgi complex and basolateral surface of the enterocytes suggests

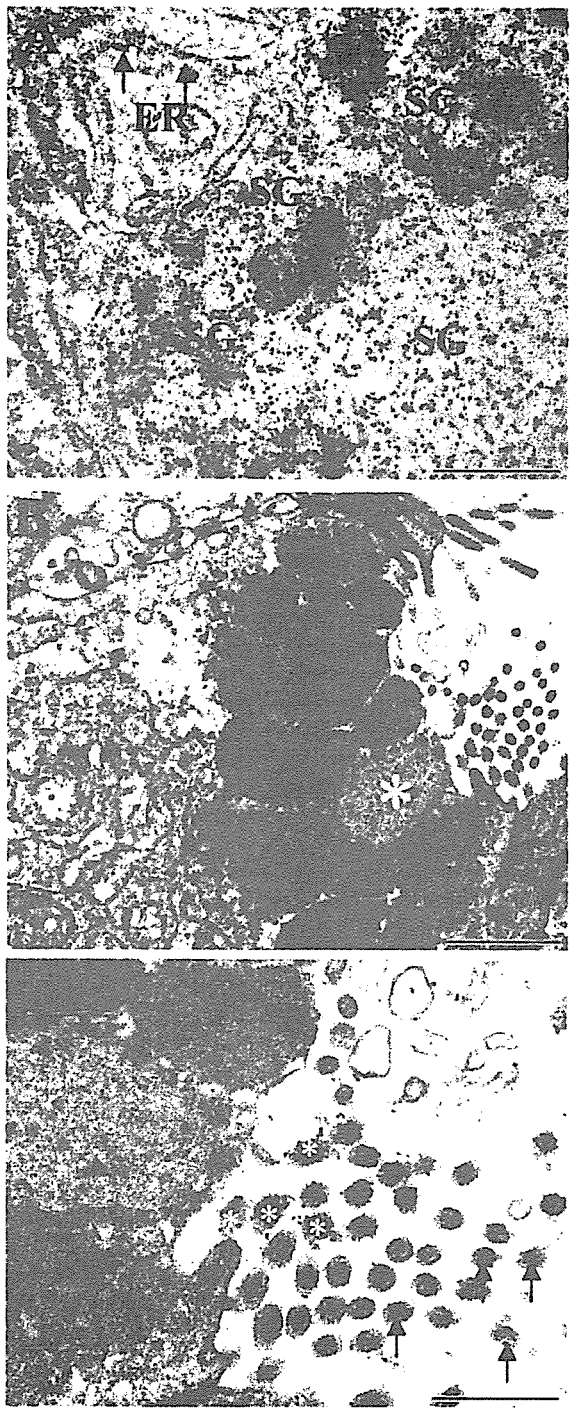

FIGURE 4: Immunogold localization of intelectin in goblet cells. (A) Electron micrograph showing labeling of endoplasmic reticulum (ER) membranes (indicated by arrows) adjacent to a heavily labeled region of secretory granules (SG). (B) Apical region of a goblet cell in the crypt region, containing several heavily labeled secretory granules. One granule at the cell surface (marked with an asterisk) is lighter in color than its neighboring granules and contains much less labeling, indicating an ongoing degranulation. (C) The microvilli of enterocytes in the proximity of the degranulating goblet cell (marked with asterisks) are decorated with gold particles, indicating a deposition of intelectin. By comparison, microvilli farther from the goblet cell show no or little labeling (arrows). Bars are 0.5 (A and C) and 1 μm (B).

that intelectin may also, at least in part, be synthesized and exocytosed by the enterocytes themselves.

Identification of Intelectin in Microvillar Superrafts. A superraft analysis of microvillar membrane vesicles was next performed to characterize the brush border association of intelectin. We have previously characterized a superraft fraction derived from pig intestinal microvillar DRMs by sequential extractions with Triton X-100, first at room temperature and then at 37 °C, finally yielding a membranous fraction that resists solubilization at physiological temperature (*7*). This microvillar subfraction was particularly enriched in glycolipids and the β-galactoside-recognizing lectin galectin-4, and the latter was proposed to function as a core lipid raft stabilizer/organizer for other, more loosely raft-associated proteins.

Figure 6 shows a superraft analysis of mouse microvillar membranes, prepared by the divalent cation precipitation method that yields a homogeneous population of closed, outside-out membrane vesicles (*30*). Two bands of ~15−20 kDa were by far the most predominant components of the superraft fraction, and both were identified by MALDI-TOF analysis as fragments of galectin-4 (36 kDa). Galectin-4 is a divalent lectin that contains two separate carbohydrate recognition domains each of ~130 amino acids, connected by a smaller linker peptide (*6*, *38*). None of the sequence-matching peptides obtained for either of the two bands (18 peptides in all) were localized to the central linker region, indicating that the full-length galectin-4 in the mouse is effectively cleaved into two separate carbohydrate recognition domains (data not shown). Mouse microvillar glycosylphosphatidylinositol-anchored alkaline phosphatase (~70 kDa) was highly enriched in the superraft fraction, as previously observed in the pig (*7*). Annexin A2 is another raft-associated protein that is present in intestinal microvillar as well as intracellular membranes (*39*), and although clearly detectable in superrafts, it was not enriched in this fraction relative to the microvillar- and Mg^{2+}-precipitated membranes (Figure 5), indicating that it does not belong to the core components of the lipid raft microdomains. In contrast, a band of 35−40 kDa was highly enriched in the superraft fraction, and by MALDI-TOF analysis, six sequence-matching peptides identified this protein as intelectin (peptide molecular mass of 35 kDa). Previously, a comparison of molecular mass values of hIntL under reducing and nonreducing conditions has indicated that the native intelectin is a homotrimer (*20*). The presence of intelectin in the microvillar superraft fraction therefore implies that it may serve as a lipid raft organizer/stabilizer like galectin-4 by cross-linking lipid and protein glycoconjugates at the brush border membrane.

Immunogold Localization of Intelectin in Microvillar Vesicles and Superrafts. Morphologically, an intestinal microvillar fraction appears as closed, outside-out membrane vesicles with a diameter of ~100 nm (Figure 7A). Superrafts also form vesicle-like structures, albeit of a more heterogeneous composition, and in addition, tubular or rodlike membranes are seen (Figure 7B), as previously described (*7*). Both microvillar vesicles and superrafts were prominently labeled by the intelectin antibody, confirming the presence of intelectin in the enterocyte brush border as well as the biochemical identification of intelectin as a major component of superrafts (Figure 6). The labeling density of

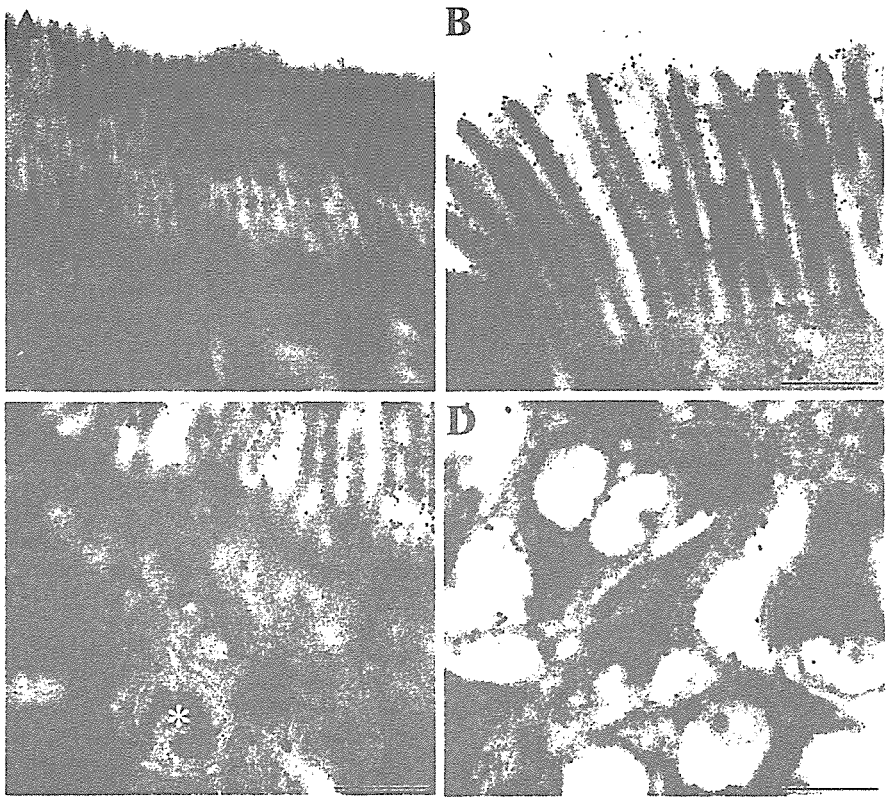

FIGURE 5: Immunogold localization of intelectin in enterocytes. (A) Electron micrograph showing the brush border of two neighboring enterocytes of which the one to the right is intensely labeled and the one to the left only weakly labeled. (B) Aggregates of gold particles are frequently seen in invaginations between microvilli (arrows) and in vesicle-like structures in the proximity of the apical cell surface (arrowheads). (C) A multivesicular body in the subapical region (asterisk) heavily labeled by gold particles. (D) Labeling of membranes in the Golgi complex region. Bars are 1 (A) and 0.5 μm (B–D).

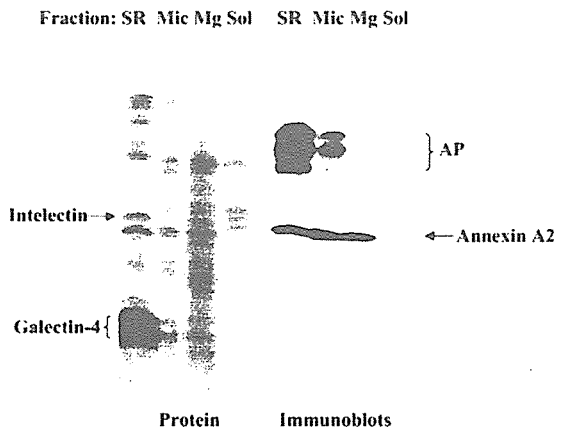

FIGURE 6: Intelectin is enriched in superrafts from microvillar membranes. Mouse intestinal mucosa was fractionated into microvillar membranes (Mic), Mg^{2+}-precipitated (basolateral and intracellular) membranes (Mg), soluble proteins (Sol), and microvillar superraft (SR) membranes prepared as described in Materials and Methods. After SDS–PAGE and transfer onto Immobilon, alkaline phosphatase (AP) and annexin A2 were visualized by immunoblotting. After protein staining, a distinct band of 35–40 kDa and two intense bands of 15–20 kDa were carefully excised and submitted to MALDI-TOF analysis. The former was identified as intelectin and the latter as fragments of galectin-4.

the superraft membranes was not much different from that of the microvillar membranes, despite the enrichment seen in SDS–PAGE. Most likely, this is explained by a previous observation that raft lipids (cholesterol and glycolipids) are only moderately enriched in superrafts (~1.2–1.5-fold), indicating that it is mainly proteins and not lipids that are removed from the membranes by the sequential detergent extractions at increasing temperatures (*7*).

Binding and Uptake of Lactoferrin. Human lactoferrin is known to bind to the mouse LfR (*40*), and as shown in Figure 8A, this ligand bound to the lumenal surface of intestinal explants cultured for 30 min at 4 °C. The entire brush border was labeled with lactoferrin with punctate strong labeling occasionally seen at the tip of the microvilli. When the explant was cultured for 30 min at 37 °C, a temperature that permits endocytosis, the punctate labeling was much more pronounced, and some of the clustering appeared below the apical surface (Figure 8B). No labeling below the subapical region of the enterocytes was detectable.

Immunogold electron microscopy confirmed the binding of lactoferrin to the enterocyte brush border with clustering at the tip of the microvilli at 4 °C (Figure 9A). No intracellular labeling was detected at this temperature. At 37 °C, the clusters of gold particles typically appeared at the base of the microvilli (Figure 9B) and in subapical endosomal structures (Figure 9C). This pattern of labeling resembles that of intelectin (Figure 5), suggesting that lactoferrin, after binding to the brush border, is clustered and eventually internalized together with its receptor.

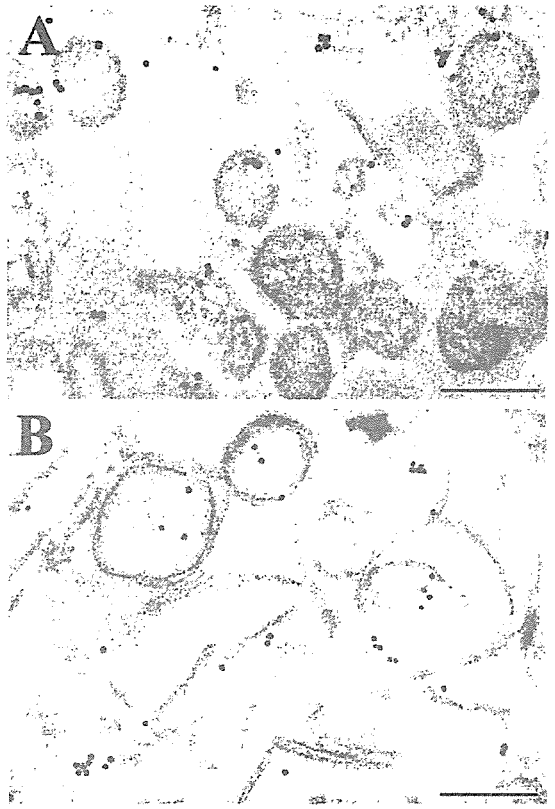

FIGURE 7: Immunogold localization of intelectin in microvillar vesicles and superrafts. Electron micrographs showing intelectin labeling of microvillar membrane vesicles (A) and superraft membranes (B). Bars are 100 nm.

DISCUSSION

The results of this work demonstrate that intelectin is present in both Paneth and goblet cells as well as in the enterocyte brush border. The intense immunolabeling observed in the secretory granules of the former two cell types agrees well with the initial identification of intelectin in Paneth cells of the crypts (*19*) and the observed inducible expression of the intelectin-2 isoform in goblet cells of the BALB/c mouse (*21*, *22*), but to our knowledge, localization of intelectin in the enterocyte brush border has not previously been reported. In contrast, LfR has long been recognized as a brush border protein (*40*−*42*), whereas its secretion from neither Paneth nor goblet cells, to our knowledge, has been reported. The immunofluorescence labeling pattern indicated that the brush border is indeed the major site of intelectin deposition, but most likely, the brush border intelectin originates, at least in part, from goblet cells. Like lumenally secreted lectin-like anti-glycosyl antibodies (*16*), soluble goblet cell-derived intelectin most likely associates with lipid rafts in the enterocyte brush border due to the high density of its carbohydrate ligands in these microdomains. This interpretation is supported by a mouse in situ hybridization database showing the level of intelectin expression to be highest in the crypt region, which harbors the largest population of goblet cells, although expression in villi is also detectable (*43*). However, previous work on LfR indicates that the enterocytes themselves syntesize and transport the protein to the apical surface. Thus, in the enterocyte-like

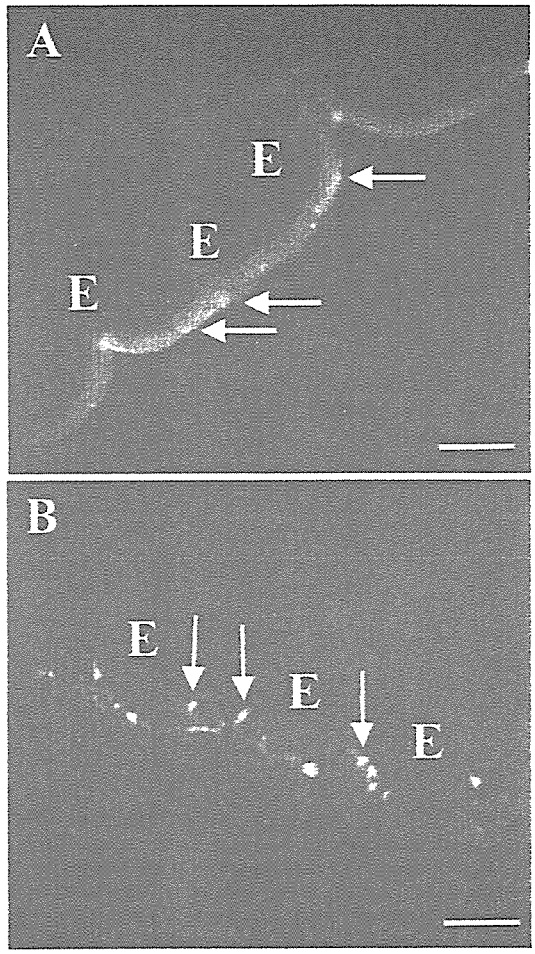

FIGURE 8: Binding and uptake of lactoferrin by enterocytes. Mouse small intestinal explants were cultured for 30 min in the presence of 0.5 mg/mL lactoferrin at 4 (A) or 37 °C (B). After being washed in fresh MEM medium, the explants were fixed in 4% paraformaldehyde and prepared for immunofluorescence microscopy as described in Materials and Methods. At 4 °C, lactoferrin bound to the entire lumenal surface with punctate of bright fluorescence aligned at the rim of the brush border (arrows). At 37 °C, the punctate lactoferrin labeling was more pronounced and in some cases appeared below the apical surface (arrows). E denotes enterocytes. Bars are 10 μm.

Caco-2 cell line which expresses low levels of LfR, a major part of the protein was released by phosphatidylinositol-specific phospholipase C, indicating a membrane insertion by a GPI anchor (*25*). In support of this observation, a hydrophobic consensus sequence for attachment of a GPI anchor is present in the C-terminus of the molecule (*25*). Enterocytes synthesize a number of brush border GPI-anchored proteins, including alkaline phosphatase (*44*) and melanotransferrin (*45*), showing that this cell type harbors the enzymes required for anchorage of GPI in the endoplasmic reticulum, but whether they synthesize a GPI-anchored form of the lactoferrin receptor remains to be investigated further. The distinct immunogold labeling over the Golgi complex membranes observed in this work at least suggests that enterocytes themselves contribute to the overall expression of intelectin in the brush border. Interestingly, melanotransferrin, expressed in the intestine only during fetal and neonatal life and presumably involved in uptake of iron, was

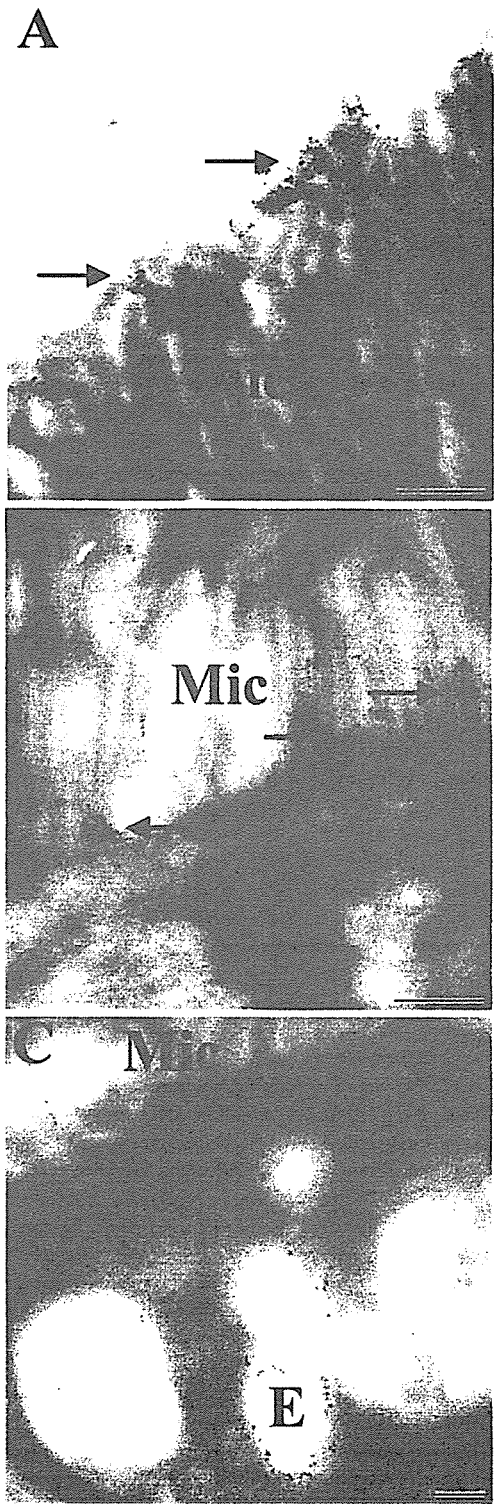

FIGURE 9: Immunogold localization of bound and endocytosed lactoferrin. Immunogold electron micrographs of the lactoferrin binding and uptake experiments shown in Figure 8. (A) After 30 min at 4 °C, clusters of gold particles (arrows) were seen at the tip of the microvilli (Mic). (B and C) After 30 min at 37 °C, the clusters of particles were present near the base of the microvilli (arrows) and in subapical endosomes (E). Bars are 0.5 (A and B) and 0.2 μm (C).

observed in apical endocytic vacuoles and tubulo-vesicular structures, suggesting that it undergoes internalization from the apical surface (*45*). The LfR also exhibits an age-dependent expression profile (*25*), but there are contradictory reports about whether it is endocytosed from the brush border. Thus, whereas lactoferrin was not internalized from the surface of HT 29-D4 cells (*46*), specific uptake from the apical surface of Caco-2 cells was demonstrated (*47*). Interestingly, the lactoferrin that is taken up is localized to the nuclei, in contrast to transferrin which accumulated in the cytoplasm (*47*). This work strongly argues that lactoferrin binds to the enterocyte brush border, and that at least a fraction of it concentrates in hot spots that are taken up by the absorptive cell. Clearly, further work is needed to characterize this lactoferrin internalization in greater detail, but we speculate that the apparently conflicting results may reflect the presence of two different molecular forms of intelectin/LfR: a GPI-anchored, internalization-competent form and a soluble secretory form that is capable of binding lactoferrin and other ligands but is unable to mediate cellular uptake. A putative role of internalized lactoferrin in the nucleus is to act as a transcription factor, possibly stimulating synthesis of proinflammatory cytokine interleukin 18 in the enhancement of the immune system (*24*, *48*, *49*), and at the cell surface, lactoferrin is able to exert a bacteriostatic effect by withholding iron (*50*, *51*). Along these lines, a differential expression of a GPI-anchored form of LfR made by enterocytes, and a soluble form, made by Paneth and goblet cells, could be a simple mechanism for ensuring the delivery of lactoferrin to its two different sites of function.

A common functional theme in the roles ascribed to intelectin and LfR is the mucosal protection against lumenal pathogenic microorganisms and parasites. Here, the essential lactoferrin-independent property seems to be the ability to bind a broad range of carbohydrate structures, including galactofuranose, which is contained in bacterial carbohydrate chains but is lacking in the mammalian host organism (*20*). Soluble defense lectins are generally thought to function as agglutinins, but intelectin reportedly appears to lack agglutination properties, possibly because this lectin does not form noncovalent multimers (*20*). However, the prominent anti-intelectin labeling of the brush border demonstrated in this work is suggestive of an alternative mucosal defense mechanism. Thus, glycolipids with terminal galactose residues, including galactosylceramide, lactosylceramide, and GM_1, are plentiful at the lumenal surface (*3*, *7*), and as shown in this work, much of the soluble intelectin secreted by goblet and Paneth cells is deposited here rather than released freely into the gut lumen. As observed recently for anti-glycosyl antibodies (*16*), intelectin may protect the brush border glycolipids from acting as pathogen receptors. In addition, like divalent galectin-4, trivalent intelectin should be capable of cross-linking lipid and protein glycoconjugates and thereby contribute to formation of stable microdomains, as exemplified by superrafts. In addition, this architecture helps to minimize the loss of digestive enzymes to the gut lumen (*7*), an important rescuing function for enzymes with reported half-lives as short as 5−8 h (*52*).

Very recently, the genomic structure of human omentin, a putative, new adipocytokine expressed in omental adipose tissue, was reported and revealed to be 100% identical to that of human intelectin (*53*). Interestingly, omentin expres-

sion was weak or absent in the majority of tissue probes obtained from patients suffering from Crohn's disease, suggesting a role for the protein in the defense against intestinal bacterial translocation in the context of this disease. This observation is consistent with the multiple defense functions attributed to intelectin/lactoferrin receptor and underscores the general importance of this protein.

ACKNOWLEDGMENT

Lise-Lotte Niels-Christiansen and Lissi Immerdal are thanked for expert technical assistance.

REFERENCES

1. Trier, J. S. (1968) Morphology of the epithelium of the small intestine, *Code C.F. Handbook of Physiology: Alimentary Canal*, Vol. 6, pp 1125−1176, American Physiological Society, Washington, DC.
2. Sansonetti, P. J. (2004) War and peace at mucosal surfaces, *Nat. Rev. Immunol. 4*, 953−964.
3. Christiansen, K., and Carlsen, J. (1981) Microvillus membrane vesicles from pig small intestine. Purity and lipid composition, *Biochim. Biophys. Acta 647*, 188−195.
4. Hauser, H., Howell, K., Dawson, R. M., and Bowyer, D. E. (1980) Rabbit small intestinal brush border membrane preparation and lipid composition, *Biochim. Biophys. Acta 602*, 567−577.
5. Barondes, S. H., Cooper, D. N., Gitt, M. A., and Leffler, H. (1994) Galectins. Structure and function of a large family of animal lectins, *J. Biol. Chem. 269*, 20807−20810.
6. Huflejt, M. E., and Leffler, H. (2004) Galectin-4 in normal tissues and cancer, *Glycoconjugate J. 20*, 247−255.
7. Braccia, A., Villani, M., Immerdal, L., Niels-Christiansen, L. L., Nystrom, B. T., Hansen, G. H., and Danielsen, E. M. (2003) Microvillar membrane microdomains exist at physiological temperature: Role of galectin-4 as lipid raft stabilizer revealed by "superrafts", *J. Biol. Chem. 278*, 15679−15684.
8. Danielsen, E. M., and Hansen, G. H. (2003) Lipid rafts in epithelial brush borders: Atypical membrane microdomains with specialized functions, *Biochim. Biophys. Acta 1617*, 1−9.
9. Hansen, G. H., Dalskov, S. M., Rasmussen, C. R., Immerdal, L., Niels-Christiansen, L. L., and Danielsen, E. M. (2005) Cholera Toxin Entry into Pig Enterocytes Occurs via a Lipid Raft- and Clathrin-Dependent Mechanism, *Biochemistry 44*, 873−882.
10. Duncan, M. J., Shin, J. S., and Abraham, S. N. (2002) Microbial entry through caveolae: Variations on a theme, *Cell. Microbiol. 4*, 783−791.
11. Manes, S., del Real, G., and Martinez, A. (2003) Pathogens: Raft hijackers, *Nat. Rev. Immunol. 3*, 557−568.
12. Rosenberger, C. M., Brumell, J. H., and Finlay, B. B. (2000) Microbial pathogenesis: Lipid rafts as pathogen portals, *Curr. Biol. 10*, R823−R825.
13. Shin, J. S., and Abraham, S. N. (2001) Caveolae as portals of entry for microbes, *Microbes Infect. 3*, 755−761.
14. Brandtzaeg, P., and Johansen, F. E. (2005) Mucosal B cells: Phenotypic characteristics, transcriptional regulation, and homing properties, *Immunol. Rev. 206*, 32−63.
15. Pazur, J. H., Dresher, K. L., and Forsberg, L. S. (1978) Anti-glycosyl antibodies. Two sets of isoantibodies with specificity for different carbohydrate moieties of the same glycosyl antigen, *J. Biol. Chem. 253*, 1832−1837.
16. Hansen, G. H., Pedersen, E. D., Immerdal, L., Niels-Christiansen, L. L., and Danielsen, E. M. (2005) Anti-glycosyl antibodies in lipid rafts of the enterocyte brush border: A possible host defense against pathogens, *Am. J. Physiol. 289*, G1100−G1107.
17. Roberson, M. M., and Barondes, S. H. (1982) Lectin from embryos and oocytes of *Xenopus laevis*. Purification and properties, *J. Biol. Chem. 257*, 7520−7524.
18. Nishihara, T., Wyrick, R. E., Working, P. K., Chen, Y. H., and Hedrick, J. L. (1986) Isolation and characterization of a lectin from the cortical granules of *Xenopus laevis* eggs, *Biochemistry 25*, 6013−6020.
19. Komiya, T., Tanigawa, Y., and Hirohashi, S. (1998) Cloning of the novel gene intelectin, which is expressed in intestinal paneth cells in mice, *Biochem. Biophys. Res. Commun. 251*, 759−762.
20. Tsuji, S., Uehori, J., Matsumoto, M., Suzuki, Y., Matsuhisa, A., Toyoshima, K., and Seya, T. (2001) Human intelectin is a novel soluble lectin that recognizes galactofuranose in carbohydrate chains of bacterial cell wall, *J. Biol. Chem. 276*, 23456−23463.
21. Pemberton, A. D., Knight, P. A., Wright, S. H., and Miller, H. R. (2004) Proteomic analysis of mouse jejunal epithelium and its response to infection with the intestinal nematode, *Trichinella spiralis*, *Proteomics 4*, 1101−1108.
22. Pemberton, A. D., Knight, P. A., Gamble, J., Colledge, W. H., Lee, J. K., Pierce, M., and Miller, H. R. (2004) Innate BALB/c enteric epithelial responses to *Trichinella spiralis*: Inducible expression of a novel goblet cell lectin, intelectin-2, and its natural deletion in C57BL/10 mice, *J. Immunol. 173*, 1894−1901.
23. Datta, R., deSchoolmeester, M. L., Hedeler, C., Paton, N. W., Brass, A. M., and Else, K. J. (2005) Identification of novel genes in intestinal tissue that are regulated after infection with an intestinal nematode parasite, *Infect. Immun. 73*, 4025−4033.
24. Suzuki, Y. A., Lopez, V., and Lonnerdal, B. (2005) Mammalian lactoferrin receptors: Structure and function, *Cell. Mol. Life Sci. 62*, 2560−2575.
25. Suzuki, Y. A., Shin, K., and Lonnerdal, B. (2001) Molecular cloning and functional expression of a human intestinal lactoferrin receptor, *Biochemistry 40*, 15771−15779.
26. Danielsen, E. M., Sjostrom, H., Noren, O., Bro, B., and Dabelsteen, E. (1982) Biosynthesis of intestinal microvillar proteins. Characterization of intestinal explants in organ culture and evidence for the existence of pro-forms of the microvillar enzymes, *Biochem. J. 202*, 647−654.
27. Slot, J. W., and Geuze, H. J. (1985) A new method of preparing gold probes for multiple-labeling cytochemistry, *Eur. J. Cell Biol. 38*, 87−93.
28. Hansen, G. H., Wetterberg, L. L., Sjostrom, H., and Noren, O. (1992) Immunogold labelling is a quantitative method as demonstrated by studies on aminopeptidase N in microvillar membrane vesicles, *Histochem. J. 24*, 132−136.
29. Hansen, G. H., Niels-Christiansen, L. L., Immerdal, L., Hunziker, W., Kenny, A. J., and Danielsen, E. M. (1999) Transcytosis of immunoglobulin A in the mouse enterocyte occurs through glycolipid raft- and rab17-containing compartments, *Gastroenterology 116*, 610−622.
30. Booth, A. G., and Kenny, A. J. (1974) A rapid method for the preparation of microvilli from rabbit kidney, *Biochem. J. 142*, 575−581.
31. Brown, D. A., and Rose, J. K. (1992) Sorting of GPI-anchored proteins to glycolipid-enriched membrane subdomains during transport to the apical cell surface, *Cell 68*, 533−544.
32. Danielsen, E. M. (1995) Involvement of detergent-insoluble complexes in the intracellular transport of intestinal brush border enzymes, *Biochemistry 34*, 1596−1605.
33. Laemmli, U. K. (1970) Cleavage of structural proteins during the assembly of the head of bacteriophage T4, *Nature 227*, 680−685.
34. Lee, J. K., Buckhaults, P., Wilkes, C., Teilhet, M., King, M. L., Moremen, K. W., and Pierce, M. (1997) Cloning and expression of a *Xenopus laevis* oocyte lectin and characterization of its mRNA levels during early development, *Glycobiology 7*, 367−372.
35. Tang, Q. J., Tao, K. Z., Yun, L., Sun, X. J., Geng, M. Y., and Jiang, C. L. (2005) Immunocytochemical localization of secretory component in Paneth cell secretory granules: Rat Paneth cells participate in acquired immunity, *J. Mol. Histol. 36*, 331−335.
36. Erlandsen, S. L., Parsons, J. A., and Taylor, T. D. (1974) Ultrastructural immunocytochemical localization of lysozyme in the Paneth cells of man, *J. Histochem. Cytochem. 22*, 401−413.
37. Speece, A. J. (1964) Histochemical distribution of lysozyme activity in organs of normal mice and radiation chimeras, *J. Histochem. Cytochem. 12*, 384−391.
38. Cooper, D. N. (2002) Galectinomics: Finding themes in complexity, *Biochim. Biophys. Acta 1572*, 209−231.
39. Danielsen, E. M., van Deurs, B., and Hansen, G. H. (2003) "Nonclassical" secretion of annexin A2 to the lumenal side of the enterocyte brush border membrane, *Biochemistry 42*, 14670−14676.
40. Hu, W. L., Mazurier, J., Sawatzki, G., Montreuil, J., and Spik, G. (1988) Lactotransferrin receptor of mouse small-intestinal brush border. Binding characteristics of membrane-bound and Triton X-100-solubilized forms, *Biochem. J. 249*, 435−441.
41. Kawakami, H., and Lonnerdal, B. (1991) Isolation and function of a receptor for human lactoferrin in human fetal intestinal brush-border membranes, *Am. J. Physiol. 261*, G841−G846.

42. Suzuki, Y. A., and Lonnerdal, B. (2004) Baculovirus expression of mouse lactoferrin receptor and tissue distribution in the mouse, *BioMetals 17*, 301−309.
43. Olsen, L., Hansen, M., Ekstrom, C. T., Troelsen, J. T., and Olsen, J. (2004) CVD: The intestinal crypt/villus in situ hybridization database, *Bioinformatics 20*, 1327−1328.
44. Lowe, M., Strauss, A. W., Alpers, R., Seetharam, S., and Alpers, D. H. (1990) Molecular cloning and expression of a cDNA encoding the membrane-associated rat intestinal alkaline phosphatase, *Biochim. Biophys. Acta 1037*, 170−177.
45. Danielsen, E. M., and van Deurs, B. (1995) A transferrin-like GPI-linked iron-binding protein in detergent-insoluble noncaveolar microdomains at the apical surface of fetal intestinal epithelial cells, *J. Cell Biol. 131*, 939−950.
46. Roiron-Lagroux, D., and Figarella, C. (1990) Evidence for a different mechanism of lactoferrin and transferrin translocation on HT 29-D4 cells, *Biochem. Biophys. Res. Commun. 170*, 837−842.
47. Ashida, K., Sasaki, H., Suzuki, Y. A., and Lonnerdal, B. (2004) Cellular internalization of lactoferrin in intestinal epithelial cells, *BioMetals 17*, 311−315.
48. Nichols, B. L., McKee, K. S., Henry, J. F., and Putman, M. (1987) Human lactoferrin stimulates thymidine incorporation into DNA of rat crypt cells, *Pediatr. Res. 21*, 563−567.
49. Wang, W. P., Iigo, M., Sato, J., Sekine, K., Adachi, I., and Tsuda, H. (2000) Activation of intestinal mucosal immunity in tumor-bearing mice by lactoferrin, *Jpn. J. Cancer Res. 91*, 1022−1027.
50. Valenti, P., and Antonini, G. (2005) Lactoferrin: An important host defence against microbial and viral attack, *Cell. Mol. Life Sci. 62*, 2576−2587.
51. Legrand, D., Elass, E., Carpentier, M., and Mazurier, J. (2005) Lactoferrin: A modulator of immune and inflammatory responses, *Cell. Mol. Life Sci. 62*, 2549−2559.
52. Dudley, M. A., Hachey, D. L., Quaroni, A., Hutchens, T. W., Nichols, B. L., Rosenberger, J., Perkinson, J. S., Cook, G., and Reeds, P. J. (1993) In vivo sucrase-isomaltase and lactase-phlorizin hydrolase turnover in the fed adult rat, *J. Biol. Chem. 268*, 13609−13616.
53. Schaffler, A., Neumeier, M., Herfarth, H., Furst, A., Scholmerich, J., and Buchler, C. (2005) Genomic structure of human omentin, a new adipocytokine expressed in omental adipose tissue, *Biochim. Biophys. Acta 1732*, 96−102.

BI060570X

Available online at www.sciencedirect.com
SCIENCE DIRECT
Journal of Controlled Release 113 (2006) 271 – 278
journal of controlled release
www.elsevier.com/locate/jconrel
GENE DELIVERY

The short consensus repeats 1 and 2, not the cytoplasmic domain, of human CD46 are crucial for infection of subgroup B adenovirus serotype 35

Fuminori Sakurai [a], Sayaka Murakami [a,b], Kenji Kawabata [a], Naoki Okada [c], Akira Yamamoto [b], Tsukasa Seya [d], Takao Hayakawa [e], Hiroyuki Mizuguchi [a,c,*]

[a] *Laboratory of Gene Transfer and Regulation, National Institute of Biomedical Innovation, Osaka, 567-0085, Japan*
[b] *Department of Biopharmaceutics, Kyoto Pharmaceutical University, Kyoto, 607-8414, Japan*
[c] *Graduate School of Pharmaceutical Sciences, Osaka University, Osaka, 565-0871, Japan*
[d] *Department of Microbiology and Immunology, Graduate School of Medicine, Hokkaido University, Sapporo, 060-8638, Japan*
[e] *Pharmaceuticals and Medical Devices Agency, Tokyo, 100-0013, Japan*

Received 21 October 2005; accepted 8 May 2006
Available online 21 June 2006

Abstract

Human CD46 (membrane cofactor protein) has recently been identified to be an attachment receptor for subgroup B adenoviruses (Ads); however, the precise interaction between human CD46 and subgroup B Ads are just beginning to be understood. In this study, to characterize the interaction between human CD46 and subgroup B Ads, varieties of mutant CD46 were tested for their ability to act as a receptor for Ad serotype 35 (Ad35), which belongs to subgroup B. In addition, we determined Ad35 vector-mediated transgene expression and cellular uptake of Ad35 vectors in the presence of a set of anti-CD46 antibodies. Our data demonstrated that the short consensus repeats (SCRs) 1 and 2 in human CD46 are important for interaction with Ad35, whereas the cytoplasmic domain of human CD46 was found not to be required for the function as an Ad35 receptor. Rather, a complete deletion of the cytoplasmic domain of human CD46 increased the transduction efficiencies of Ad35 vectors. This information should help in elucidation of the mechanism of subgroup B Ad infection, as well in the improvement of the subgroup B Ad vectors.

Keywords: Adenovirus serotype 35 vector; CD46; Short consensus repeat; Cytoplasmic tail; Gene therapy

1. Introduction

Human adenoviruses (Ads) compose a large family of non-enveloped, double-stranded DNA viruses that are a significant cause of acute respiratory, gastrointestinal, and ocular infections in humans. So far, at least 51 serotype Ads have been identified and classified into six distinct subgroups (A–F) [1,2]. Among them, subgroup B is further subdivided into subspecies B1 and B2 on the basis of various biophysical and biochemical criteria. Among the 51 human Ad serotypes, the Ad vector most commonly used for gene transfer is composed of Ad serotype 5 (Ad5), which belongs to subgroup C. Ad5 vectors are very powerful and useful vehicles, but recent studies have revealed that they also have some disadvantages, such as high seroprevalence toward Ad5 in adult populations and low infection activity in cells lacking a primary receptor for Ad5, coxsackievirus and adenovirus receptor (CAR). On the other hand, subgroup B Ads have unique properties that are distinct from those of other subgroup Ads, and that are highly attractive features as a framework for alternative gene delivery vehicles. First, subgroup B Ads have been identified as having lower prevalence than the Ads of other subgroups. The seroprevalences toward most subgroup B Ads is less than 20% in healthy blood donors, while more than 70% of serum samples from healthy donors are positive for anti-Ad5 antibody [3]. This indicates that transduction with Ad vectors based on subgroup B is unlikely to be inhibited by preexisting anti-Ad antibodies. Second, subgroup B Ads utilize human CD46 (membrane cofactor protein) as a cellular receptor for infection [4,5], while other subgroup Ads recognize CAR. Human CD46 is ubiquitously expressed in human cells, suggesting that subgroup

* Corresponding author. Laboratory of Gene Transfer and Regulation, National Institute of Biomedical Innovation, 7-6-8 Asagi, Saito, Ibaragi-City, Osaka, 567-0085, Japan. Tel.: +81 72 641 9815; fax: +81 72 641 9816.
E-mail address: mizuguch@nibio.go.jp (H. Mizuguchi).

0168-3659/$ - see front matter © 2006 Elsevier B.V. All rights reserved.
doi:10.1016/j.jconrel.2006.05.007

B Ad vectors would have a broad tropism for human cells. We have previously developed an Ad vector composed of Ad serotype 35 (Ad35), which belongs to subgroup B [6,7], and have demonstrated that Ad35 vectors exhibit a wider tropism for human cells, including CAR-negative cells, than Ad5 vectors [7].

Human CD46 is a type I transmembrane glycoprotein expressed in almost all human cells, except for erythrocytes. Human CD46 is composed of four cysteine-rich short consensus repeats (SCRs), a serine–threonine–proline-rich (STP) region, a short region of unknown function, a hydrophobic transmembrane domain, and a carboxy-terminal cytoplasmic domain. Alternative splicing in the STP region and the cytoplasmic domain gives rise to four major isoforms of human CD46 (BC1, BC2, C1, and C2). All the isoforms function as cofactors for the plasma serine protease factor I by binding to the complement factors C3b and C4b deposited on self tissue [8,9]. By promoting the proteolytic degradation of these factors, these isoforms protect the cells from complement attack [10,11]. In addition to this function, human CD46 has been identified to be a receptor for several human pathogens: measles virus (MV), human herpesvirus 6 (HHV6), human subgroup B Ads, and two types of bacteria [4,5,12–15]. Among these pathogens, the interactions between human CD46 and MV, HHV6, and pathogenic *Neisseria* have been well studied. MV-binding residues are located on SCR1 and SCR2 [16,17], while SCR3 and 4 are essential for binding of HHV6 to human CD46 [18]. The cytoplasmic domain of CD46 is not required for infection of both MV and HHV6 [18,19]. However, it still remains unknown which domains in human CD46 play an important role in the interaction with subgroup B Ads. Elucidation of the interaction between subgroup B Ads and CD46 would lead to improvement of the Ad vectors that are composed of subgroup B Ads.

In this study, the transduction experiments with Ad35 vectors expressing luciferase were performed using cells expressing a variety of human CD46 mutants in order to map the domains which interact with Ad35. Furthermore, cells expressing wild-type CD46 were transduced with Ad35 vectors in the presence of monoclonal anti-human CD46 antibodies which recognize different SCRs of human CD46. Finally, involvement of the cytoplasmic domain of human CD46 with infection of Ad35 was evaluated.

2. Materials and methods

2.1. Cells and antibodies

Chinese hamster ovary (CHO) cells and CHO transformants stably expressing wild-type CD46, CD46 SCR deletion mutants [16], or cytoplasmic tail deletion mutants were grown in Ham's F-12 medium with 10% fetal bovine serum. Cytoplasmic tail deletion mutants (ΔCyt0 and ΔCyt6 mutants) were stable CHO transformants generated by the transfection of pcDNA-CD46Δ Cyt0 and pcDNA-CD46ΔCyt6 (described below) into CHO cells and selection with hygromycin (GIBCO-BRE, Rockville, MD). Monoclonal antibodies against human CD46 SCR1, E4.3, MEM-258, and J4-48 were purchased from Pharmingen (San Diego, CA), Serotec Ltd. (Oxford, United Kingdom), and Immunotech (Marseille, France), respectively. SCR2-specific antibody M177 and SCR3-specific antibody M160 were described previously [20]. The monoclonal anti-CD46 antibodies used in this study and their recognition sites are listed on Table 1.

2.2. Plasmids

The plasmid pcDNA-CD46C2, which contains the human CD46 C2 isoform gene, was constructed as follows. The cDNA of the human CD46 C2 isoform was amplified by PCR using the following primers: CD46-forward, 5′-ATG GAG CCT CCC GGC CGC CGC GAG TGT CCC-3′; CD46-reverse, 5′-CGC GGC CGC CTA TTC AGC CTC TCT GCT CTG CTG-3′. The PCR product was cloned into the *Pme*I site of pcDNA3.1-Hyg(+) (Invitrogen, Carlsbad, CA). The cDNA of the CD46 mutant lacking the cytoplasmic tail (amino acid residues 347–369) (CD46ΔCyt0) was prepared by PCR using the parent CD46 C2 cDNA as a template. The following primers were used for PCR: CD46-forward (described above); and CD46TM-reverse, 5′-GCG GCC GCT CAG TAC GGG ACA ACA CAA ATT ACT GCA AC-3′. The PCR product was cloned into the *Pme*I site of pcDNA3.1-Hyg(+), resulting in pcDNA-CD46ΔCyt0. The plasmid pcDNA-CD46ΔCyt6, which contains a human CD46 C2 isoform lacking a portion of the cytoplasmic domain (amino acid residues 352–369) (CD46ΔCyt6), was constructed in a similar manner using the following primers: CD46-forward (described above); and CD46TM6-reverse, 5′-GCG GCC GCT CAC CTC CTT TGA AGA TAT CTG TAC GGG AC-3′. The sequences of all the constructs were confirmed by DNA sequencing.

2.3. Flowcytometric analysis of CD46 expression

Several CHO cell transformants suspended in staining buffer (phosphate buffered saline (PBS) buffer containing 1% bovine serum albumin (BSA)) were incubated with mouse anti-human CD46 antibodies (E4.3, M177, and M160) for 1 h. Subsequently, the cells were reacted with phycoerythrin (PE)-labeled secondary anti-mouse IgG antibody (Pharmingen). After washing with the staining buffer, the stained cells (10^4 cells) were analyzed using a FACSCalibur and CellQuest software (Becton Dickinson, Tokyo, Japan). For evaluation of Ad35 vector-mediated downregulation of CD46, the CHO transformants were transduced with Ad35L at 3000 vector particles (VP)/cell for 1.5 h as described below. After a 1.5-h incubation, CD46 expression levels in the cells were measured using flowcytometry as described above.

Table 1
Monoclonal anti-CD46 antibodies used in this study

Anti-CD46 antibodies	Recognition domain
E4.3	SCR1
J4-48	SCR1
MEM-258	SCR1
M177	SCR2
M160	SCR3

2.4. Adenovirus vectors

Ad35 vectors expressing luciferase, Ad35L, were prepared by an improved ligation method as previously described [21]. Briefly, the luciferase-expressing Ad35 vector plasmid pAdMS4-CMVL2 was constructed by ligating I-*Ceu*I/PI-*Sce*I-digested pAdMS4 with I-*Ceu*I/PI-*Sce*I-digested pCMVL1 [22]. pAdMS4-CMVL2 was digested with *Sbf*I and the linearized DNA was transfected into VK10-9 cells (kindly provided by Dr. V. Krougliak) [23]. Ad35L were generated 10–14 days after transfection, amplified and purified as described previously [6,7]. Determination of virus particle titers was accomplished spectrophotometrically by the method of Maizel et al. [24].

2.5. Transduction experiments

CHO cells and CHO transformants stably expressing wild-type CD46 or CD46 mutants lacking SCRs or the cytoplasmic tail were seeded at 1×10^4 cells/well into a 96-well plate. On the following day, the cells were transduced with Ad35L at 3000 VP/cell for 1.5 h. Forty-eight hours later, luciferase productions in the cells were measured using a luciferase assay system (PicaGene LT2.0, Toyo Inki Co. Ltd., Tokyo, Japan).

For antibody blocking experiments, CHO transformant expressing CD46 C2 isoform, which was seeded at 1×10^4 cells/well in a 96-well plate the day before transduction, was preincubated with the medium containing anti-CD46 antibodies (E4.3, MEM-258, J4-48, M177, and M160) at the indicated concentrations at 4 °C for 1 h. Ad35L was then added at 3000 VP/cell and left for 1.5 h at 4 °C, after which the cells were washed and incubated at 37 °C. Luciferase productions in the cells were measured 48 h after transduction as described above.

2.6. Real-time quantitative PCR

CHO cells and CHO transformants were seeded at 1×10^5 cells/well into a 12-well plate. On the following day, the cells were transduced with Ad35L as described above. After a 48-h incubation, the cells were washed with PBS, harvested, and pelleted. Total DNA, including the Ad35 vector DNA, was extracted from the cells using a Tissue DNeasy Kit (Qiagen, Valencia, CA, USA). The quantitative real-time PCR was performed with 25 ng of sample DNA, 0.5 μM each primer, 0.16 μM TaqMan probe, and 25 μl of TaqMan universal PCR master mix (Applied Biosystems, Foster City, CA, USA) in a final volume of 50 μl using the ABI Prism 7000 sequence detection system (Applied Biosystems). The PCR was initially denatured at 95 °C for 10 min and then subjected to cycles of 95 °C for 15 s and 60 °C for 1 min. The reaction was carried out for 50 cycles. Primers for amplification were located in the pIX region of Ad35 genome. The sequences of the primers and probe used were as follows: forward, 5′-TGGATGGAAGACCC GTTCAA-3′; reverse, 5′-CGTCCAAAGGTGAAGAACTTA AAGT-3′; probe, 5′ FAM-CGCCAATTCTTCAACGCTGACC TATGC-TAMRA 3′. These sequences were designed using Primer Express software version 1.0 (Applied Biosystems), and it was confirmed that they amplified the products of desired size. The Ad35 vector plasmid pAdMS4 was used as a standard.

3. Results

3.1. Ad35 vector-mediated transduction on CHO transformants expressing CD46 deletion mutants

First, we examined which SCR domains of human CD46 (Fig. 1) are essential for infection of Ad35 using CHO transformants expressing CD46 deletion mutants [16]. Before the transduction experiments, CD46 expression levels and SCR deletion on CHO transformants were confirmed by flowcytometric analysis using anti-CD46 antibodies against each of the SCRs. We found the sufficient levels of CD46 mutant expression for all the clones (Fig. 2). The combined use of several anti-CD46 antibodies demonstrated that the corresponding SCR domains were properly deleted on the CHO transformants. Deletion of SCR4 on the ΔSCR4 mutant was confirmed by RT-PCR and DNA sequence, because the SCR4-specific antibody was not obtained (data not shown).

Next, transduction experiments with Ad35 vectors on CHO transformants were performed. Transduction with Ad35L in ΔSCR1 and ΔSCR2 mutants resulted in approximately 50% of the luciferase production obtained in CHO-CD46 cells, which express full-length CD46. The decreases in the transduction efficiencies in ΔSCR1 and ΔSCR2 mutants were similar. In contrast, the ΔSCR3 and ΔSCR4 mutants produced amounts of luciferase similar to those in CHO-CD46 cells after Ad35L transduction (Fig. 3). Real-time PCR analysis also demonstrated that the uptake of Ad35L was significantly reduced by 58% and by 45% in ΔSCR1 and ΔSCR2 mutants, respectively, compared with CHO-CD46 cells, in contrast, ΔSCR3 and ΔSCR4 mutants exhibited the levels of Ad35 vector uptake similar to CHO-CD46 cells (Fig. 4). These results suggested that SCR1 and 2 are involved with Ad35 infection.

3.2. Blocking of Ad35 vector infection by anti-CD46 antibodies

Next, to further examine which SCR domains in CD46 are used for Ad35 infection, several monoclonal antibodies recognizing

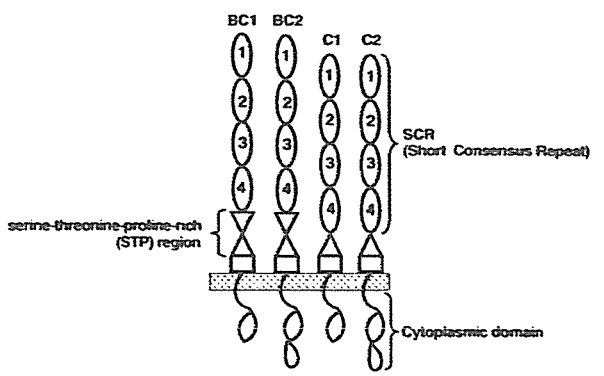

Fig. 1. A schematic diagram of human CD46. Human CD46 is ubiquitously expressed in almost all human cells mainly as four isoforms (BC1, BC2, C1, C2) that are derived via alternative splicing. Human CD46 is composed of four cysteine-rich short consensus repeats (SCRs), a serine–threonine–proline-rich (STP) region, a short region of unknown function, a hydrophobic transmembrane domain, and a carboxy-terminal cytoplasmic domain.

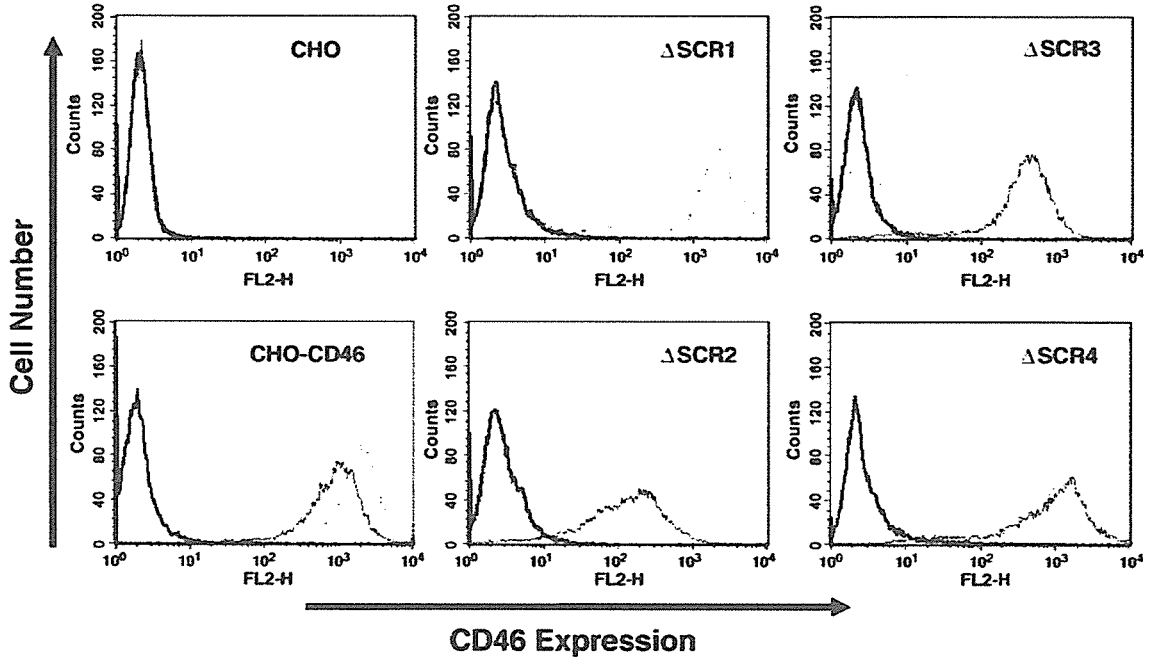

Fig. 2. Expression profiles of CD46 deletion mutants detected by monoclonal anti-CD46 antibodies. The cells were stained with anti-CD46 antibodies against SCR1 (E4.3; thin line), or SCR2 (M177; dotted line), followed by a PE-labeled secondary antibody, and subsequently analyzed by a flowcytometer. ΔSCR3 mutants were treated with anti-CD46 antibody against SCR3 (M160; dotted line) instead of M177. As a negative control, the cells were incubated with irrelevant control IgG, followed by a PE-labeled secondary antibody (thick line).

different domains of CD46 were used to block the transduction with Ad35 vectors. As shown in Fig. 5, the SCR1-specific antibody MEM-258 and the SCR2-specific antibody M177 efficiently inhibited the Ad35 vector-mediated transduction in CHO-CD46 cells. The manufacturer's information indicates that MEM-258 recognizes the SCR4 domain; however, our data indicates that MEM-258 binds to the SCR1 domain (data not shown). A recent study also reported that the epitope of MEM-258 is located in SCR1 [25]. We found that the luciferase production in the presence of both MEM-258 and M177 at 0.5 μg/ml was significantly reduced, compared with each of these antibodies alone (Fig. 5B). In contrast, the antibodies E4.3 and J4-48, which also recognize SCR1, did not decrease the luciferase production by Ad35L, suggesting that the region recognized by MEM-258, but not E4.3 and J4-48, would be involved with Ad35 infection. Decrease in the transduction efficiencies with Ad35L was not also found in the presence of the SCR3-specific antibody M160. The anti-CD46 antibodies which reduced the Ad35 vector-mediated transduction also inhibited the uptake of Ad35L by CHO-CD46 cells in a dose-dependent manner (Fig. 6). The SCR1-specific antibody MEM-258 and

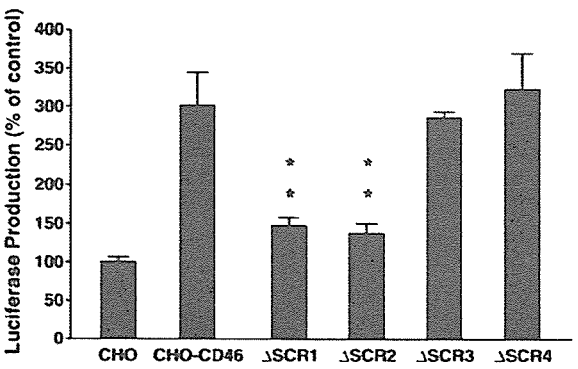

Fig. 3. Ad35L-mediated transduction in CHO cells expressing CD46 mutants lacking SCRs. The cells were transduced with Ad35L at 3000 VP/cell for 1.5 h. The luciferase productions in the cells were measured 48 h after transduction by luminescent assay. The data were normalized to the luciferase production in parental CHO cells. The absolute luciferase production in parental CHO cells was 200 pg/well. The data are expressed as the mean±S.D. (n=4). The asterisks indicate the level of significance (P<0.005 [double asterisk] for comparison with CHO-CD46 cells).

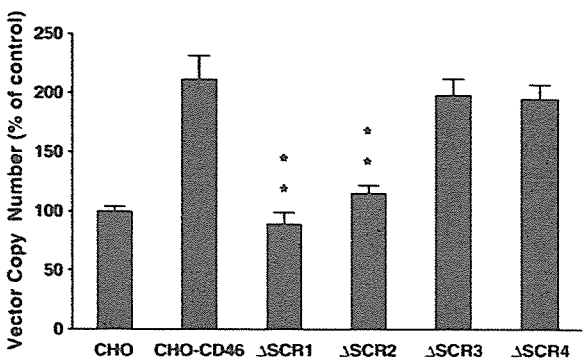

Fig. 4. Cellular uptake of Ad35L in CHO cells expressing CD46 mutants lacking SCRs. The cells were transduced with Ad35L at 3000 VP/cell for 1.5 h. The total DNA, including the vector DNA, was extracted from the cells 48 h after transduction. The copy numbers of the vector DNA were quantified by TaqMan-PCR. The data were normalized to the amounts of the vector DNA in CHO cells. The data are expressed as the mean±S.D. (n=3). The asterisks indicate the level of significance (P<0.005 [double asterisk] for comparison with CHO-CD46 cells).

the SCR2-specific antibody M177 at 5 μg/ml decreased the cellular uptake of Ad35L by 94%. These results suggest that CD46 SCR1 and SCR2 are crucial domains for Ad35 infection.

3.3. Ad35 vector-mediated transduction on CHO cells expressing mutant CD46 lacking the cytoplasmic domain

To examine whether the intracellular domain of human CD46 is required for Ad35 infection, CHO transformants expressing human CD46 C2 isoforms lacking the cytoplasmic domain, CD46ΔCYT0 and CD46ΔCYT6, were transduced with Ad35L. All of the cytoplasmic domain is deleted in CD46ΔCYT0 (amino acid residues 347–369), while CD46ΔCYT6 contains the membrane-proximal 6 amino acids of the cytoplasmic tail and lacks a portion of the cytoplasmic domain (amino acid residues 352–369)

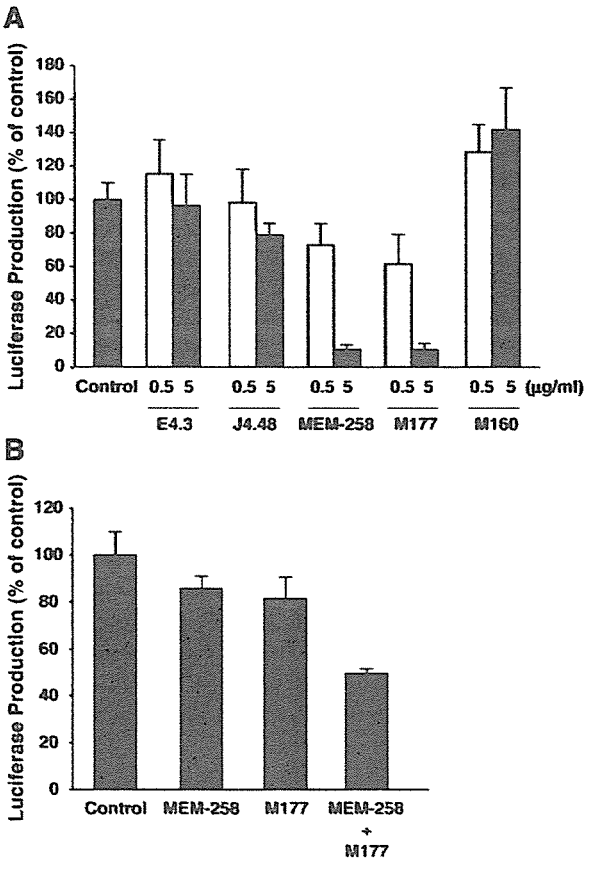

Fig. 5. Blocking of Ad35L-mediated transduction by monoclonal anti-CD46 antibodies. (A) Inhibition of Ad35L-mediated transduction by monoclonal anti-CD46 antibodies. E4.3, MEM-258, and J4-48 (recognizing SCR1), M177 (recognizing SCR2), and M160 (recognizing SCR3) were used as monoclonal anti-CD46 antibodies. CHO cells expressing wild-type CD46 were preincubated with each antibody at the indicated concentrations for 1 h and then infected with Ad35L at 3000 VP/cell. The luciferase productions in the cells were measured by luminescent assay 48 h after transduction. In control settings (Control), the cells were preincubated with medium only prior to transduction. The level of the luciferase production in control settings was almost the same as that in the presence of control mouse IgG (data not shown). (B) Combined inhibitory effect of MEM-258 and M177. The cells were preincubated with MEM-258 and/or M177 at 0.5 μg/ml. The transduction experiments were performed as described above. The data are expressed as the mean±S.D. (n=4).

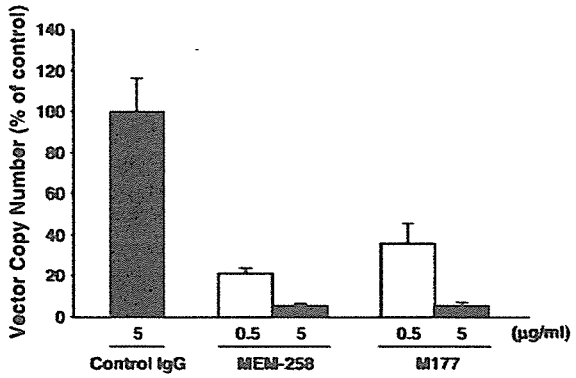

Fig. 6. Inhibition of cellular uptake of Ad35L by monoclonal anti-CD46 antibodies. CHO transformants expressing full-length CD46 were transduced with Ad35L in the presence of anti-CD46 antibody MEM-258 and M177 as described in Fig. 5. The total DNA, including the vector DNA, was extracted 48 h after transduction. The vector copy number was quantified by TaqMan-PCR. The data were normalized to the amounts of the vector DNA in CHO cells expressing full-length CD46 in the presence of control mouse IgG. The data are expressed as the mean±S.D. (n=4).

including the potential phosphorylation domain [26,27], which might be involved with various intracellular events, such as Ca^{2+} flux. The efficiency of the Ad35L-mediated transduction was similar between CHO cells expressing CD46ΔCYT6 and CHO cells expressing the full-length CD46 (Fig. 7). Furthermore, deletion of all the cytoplasmic domain significantly increased the transduction efficiency with Ad35L. These results indicate that the cytoplasmic domain of human CD46 would not be required to serve as a receptor for Ad35.

Next, we further measured the levels of CD46 expression in CHO transformants expressing wild-type CD46 or CD46ΔCYT0 following transduction with Ad35L to investigate why deletion of all the cytoplasmic domain increased the Ad35 vector-mediated transduction efficiency. The cytoplasmic domain is largely responsible to the downregulation of CD46 induced by MV [28], and

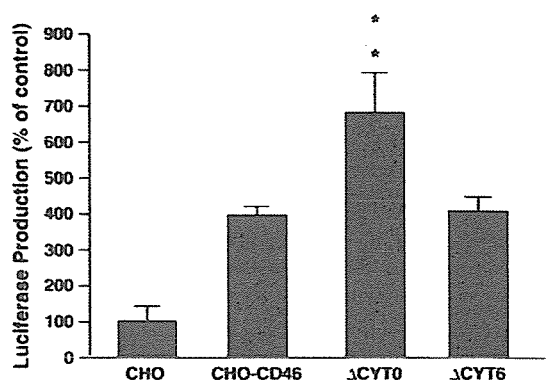

Fig. 7. Ad35L-mediated transduction in CHO cells expressing CD46 mutants lacking the cytoplasmic domain. The cells were transduced with Ad35L at 3000 VP/cells for 1.5 h. The luciferase productions in the cells were measured 48 h after transduction by luminescent assay. The data were normalized to the luciferase production in parental CHO cells. The data are expressed as the mean±S.D. (n=4). The asterisks indicate the level of significance (P<0.005 [double asterisk] for comparison with CHO-CD46).

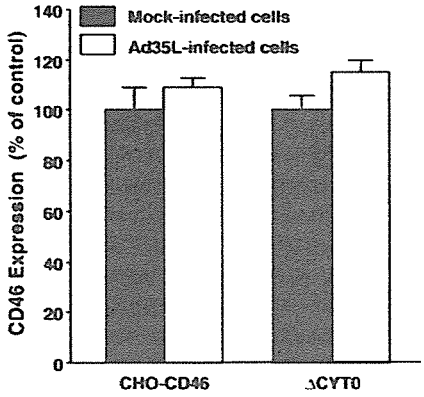

Fig. 8. CD46 expression levels in CHO transformants after infection with Ad35L. The CHO transformants expressing full-length CD46 or CD46ΔCYT0 were transduced with Ad35L at 3000 VP/cell for 1.5 h. After a 1.5-h incubation, the cells were subjected to flowcytometric analysis for measurement of CD46 expression. The data are expressed as the mean±S.D. ($n=4$).

CD46 downregulation might influence the infectivity of the viruses. Flowcytometric analysis demonstrated that CD46 downregulation did not occur in both CHO transformants expressing full-length CD46 or CD46ΔCYT0 following transduction with Ad35L (Fig. 8), suggesting that CD46 downregulation by Ad35 vectors was not involved in the increase in the transduction efficiencies of Ad35L in CHO cells expressing CD46ΔCYT0.

4. Discussion

Elucidation of the interaction between viruses and their receptors is of great importance for studies of virus pathogenicity. In addition, for the viruses that provide a framework for gene delivery vehicles, such information may help us not only to evaluate the transduction properties of virus vectors but also to improve virus vectors. In this study, CHO cells expressing CD46 deletion mutants and several monoclonal anti-CD46 antibodies were used to examine which regions are crucial for Ad35 infection. Infection experiments in cells expressing CD46 mutants lacking SCRs and blocking experiments using monoclonal anti-CD46 antibodies have already been used to determine the essential regions for infection of the pathogens recognizing CD46 in previous studies [16–18,29]. We applied this approach to elucidation of the crucial regions in CD46 for subgroup B Ad infection. The results presented herein demonstrated that the essential domains for Ad35 infection are located in SCR1 and 2, and that deletion of all the cytoplasmic domain in CD46 significantly increases Ad35 vector-mediated transduction.

Previous studies have demonstrated that MV binds to SCR1 and 2 [16,17], whereas infection of HHV6 is mediated by SCR2 and 3 [18]. Thus, SCR2 of CD46 is a crucial domain for all the human viruses utilizing CD46 (MV, HHV6, and subgroup B Ads). Moreover, SCR2-specific antibody M177 significantly inhibits the infection of all three viruses (Fig. 3) [18], suggesting that these viruses would interact with the region recognized by M177. The amino acids important for M177 binding, R69 and D70, which are located in the middle of SCR2 [30], are also present in CD46 of the cynomolgus monkey [31], which is susceptible to MV and HHV6. We also confirmed that primary cells isolated from the cynomolgus monkey were efficiently transduced with Ad35 vectors (data not shown).

Deletion of SCR1 as well as SCR2 largely decreased both the transduction efficiency and the cellular uptake of Ad35L (Figs. 3 and 4). However, SCR1-specific E4.3 and J4-48 did not significantly reduce the luciferase productions by Ad35L (Fig. 5). On the other hand, the antibody MEM-258, which also recognizes SCR1, significantly inhibited the Ad35 vector-mediated transduction and cellular uptake of Ad35L (Figs. 5 and 6). The amino acids important for binding of E4.3 and J4-48 are located on the top of SCR1 [31]. At present, it remains unclear where the epitope of MEM-258 is located within SCR1; however, the location of the epitope of MEM-258 would be different from those of E4.3 and J4-48, and would be important for Ad35 infection.

Recognition of SCR1 and 2 by Ad35 would be favorable for infection of Ad35. SCR1 and 2 are located on the upper region of CD46, leading to the decrease in electrostatic repulsion between the virus capsid and acidic cell surface proteins and the increase in attachment of Ad35 to the cell surface. Shayakhmetov and Lieber demonstrated that electrostatic repulsion between the virus capsid and cell surface is an important factor for Ad infection, especially for Ads possessing a short fiber shaft [32]. Ad35 has a shorter fiber shaft (9 nm) than Ad5 (37 nm).

During the preparation of this manuscript, two reports concerning the domains of human CD46 which interact with subgroup B Ads were published [25,33]. Gaggar et al. demonstrated that the subgroup B Ad-binding domain is located within SCR2 alone [33], while Fleischli et al. reported that the presence of both SCR1 and 2 is sufficient for infection of Ad35 and that binding of Ad35 is not confined to a single SCR domain [25]. Our data support the conclusion of Fleischli et al. The SCR2-specific antibody M177 and the deletion of SCR2 decreased Ad35 vector-mediated transduction (Figs. 3–6), suggesting that the region in SCR2 recognized by M177 would be important for interaction with Ad35. Luciferase production by Ad35L and cellular uptake of Ad35L in ΔSCR1 mutants was largely decreased, compared with CHO-CD46 cells (Figs. 3 and 4), suggesting that SCR1 would also play a role in Ad35 infection. Although the decrease in luciferase production and cellular uptake of Ad35L in the ΔSCR1 mutant might be due to conformational change of SCR2 by the deletion of SCR1, this is unlikely because the SCR2-specific antibody M177 showed positive staining in the ΔSCR1 mutant (Fig. 2). This suggests that the region recognized by M177 would hold an appropriate conformation in the ΔSCR1 mutant. Therefore, we conclude that both SCR1 and SCR2 are involved with Ad35 infection. The finding that the SCR1-specific antibody MEM-258 largely inhibited the transduction with Ad35L supports this conclusion (Figs. 5 and 6).

The cytoplasmic domain of human CD46 is not an absolute requirement in order for this protein to serve as an attachment receptor for Ad35 (Fig. 7). MV and HHV6 can also infect cells via mutant CD46 lacking the cytoplasmic domain [18,19]. However, the luciferase production was significantly increased in ΔCYT0, compared with that in CHO-CD46, in contrast, Ad35L mediated similar levels of luciferase productions in both CHO-CD46 and ΔCYT6. It remains unclear why the deletion of

the entire cytoplasmic domain of human CD46 increased the transduction efficiency, however, downregulation of CD46 was not observed in both CHO-CD46 and ΔCYT0 after transduction with Ad35L (Fig. 7). These results suggest that the increase in the transduction efficiencies of Ad35L in ΔCYT0 was not due to the lack of CD46 downregulation. One possibility for the increased transduction efficiencies in ΔCYT0 is that the amounts of CD46 which Ad35 vectors can access to would be increased by the deletion of the cytoplasmic domain. Maisner et al. demonstrated that CD46 are predominantly distributed in basolateral side of the cells and that CD46 lacking the entire cytoplasmic domain were transported to both apical and basolateral sides [34]. CD46ΔCYT0 might be more widely distributed than full-length CD46 in the CHO transformants, leading to the increase in the infection of Ad35 vectors. Another possibility is that the membrane-proximal 6 amino acids of the cytoplasmic domain in CD46 C2 isoform might contain a signal sequence for suppression of viral infection. Mouse macrophages expressing a tailless human CD46 mutant are more susceptible to MV infection than those expressing wild-type CD46 [35]. In addition to these functions of the cytoplasmic domain, the cytoplasmic domain plays important roles in immune responses through CD46, such as cytokine productions. Hirano et al. reported that the production of high levels of NO and IL-12 upon MV infection is dependent on the CD46 cytoplasmic domain [35]. Kurita-Taniguchi et al. demonstrated that intracellular phosphatase SHP-1 was found to be recruited to the cytoplasmic tail of human CD46 when human macrophages became sufficiently mature to produce IL-12 and NO in response to measles virus [36]. Therefore, the cytoplasmic domain might be involved with immune responses induced by Ad35 infection.

In summary, we demonstrated here that SCR1 and 2 of human CD46 are required for Ad35 infection, while the cytoplasmic domain of human CD46 is not crucial for an attachment receptor function for Ad35. These results offer insight into the interaction between human CD46 and subgroup B Ads, such as the internalization of Ad35 into the cells via CD46 and the crucial domain in the Ad35 fiber knob for binding to CD46.

Acknowledgements

We would like to thank Dr. Yasuko Mori (Laboratory of Virology and Vaccinology, National Institute of Biomedical Innovation, Osaka, Japan) for her advice on the cell culture. This work was supported in part by a Grants-in-Aid for Scientific Research from the Ministry of Education, Culture, Sports, Science, and Technology of Japan, and by grants for Health and Labour Sciences Research from the Ministry of Health, Labour, and Welfare of Japan.

References

[1] M.J. Havenga, A.A. Lemckert, O.J. Ophorst, M. van Meijer, W.T. Germeraad, J. Grimbergen, M.A. van Den Doel, R. Vogels, J. van Deutekom, A.A. Janson, J.D. de Bruijn, F. Uytdehaag, P.H. Quax, T. Logtenberg, M. Mehtali, A. Bout, Exploiting the natural diversity in adenovirus tropism for therapy and prevention of disease, J. Virol. 76 (2002) 4612–4620.

[2] J.C. De Jong, A.G. Wermenbol, M.W. Verweij-Uijterwaal, K.W. Slaterus, P. Wertheim-Van Dillen, G.J. Van Doornum, S.H. Khoo, J.C. Hierholzer, Adenoviruses from human immunodeficiency virus-infected individuals, including two strains that represent new candidate serotypes Ad50 and Ad51 of species B1 and D, respectively, J. Clin. Microbiol. 37 (1999) 3940–3945.

[3] R. Vogels, D. Zuijdgeest, R. van Rijnsoever, E. Hartkoorn, I. Damen, M.P. de Bethune, S. Kostense, G. Penders, N. Helmus, W. Koudstaal, M. Cecchini, A. Wetterwald, M. Sprangers, A. Lemckert, O. Ophorst, B. Koel, M. van Meerendonk, P. Quax, L. Panitti, J. Grimbergen, A. Bout, J. Goudsmit, M. Havenga, Replication-deficient human adenovirus type 35 vectors for gene transfer and vaccination: efficient human cell infection and bypass of preexisting adenovirus immunity, J. Virol. 77 (2003) 8263–8271.

[4] A. Gaggar, D.M. Shayakhmetov, A. Lieber, CD46 is a cellular receptor for group B adenoviruses, Nat. Med. 9 (2003) 1408–1412.

[5] A. Segerman, J.P. Atkinson, M. Marttila, V. Dennerquist, G. Wadell, N. Arnberg, Adenovirus type 11 uses CD46 as a cellular receptor, J. Virol. 77 (2003) 9183–9191.

[6] F. Sakurai, H. Mizuguchi, T. Hayakawa, Efficient gene transfer into human CD34+ cells by an adenovirus type 35 vector, Gene Ther. 10 (2003) 1041–1048.

[7] F. Sakurai, H. Mizuguchi, T. Yamaguchi, T. Hayakawa, Characterization of in vitro and in vivo gene transfer properties of adenovirus serotype 35 vector, Mol. Ther. 8 (2003) 813–821.

[8] T. Seya, J.R. Turner, J.P. Atkinson, Purification and characterization of a membrane protein (gp45-70) that is a cofactor for cleavage of C3b and C4b, J. Exp. Med. 163 (1986) 837–855.

[9] T. Seya, J.P. Atkinson, Functional properties of membrane cofactor protein of complement, Biochem. J. 264 (1989) 581–588.

[10] T. Seya, T. Hara, M. Matsumoto, Y. Sugita, H. Akedo, Complement-mediated tumor cell damage induced by antibodies against membrane cofactor protein (MCP, CD46), J. Exp. Med. 172 (1990) 1673–1680.

[11] D.M. Lublin, K.E. Coyne, Phospholipid-anchored and transmembrane versions of either decay-accelerating factor or membrane cofactor protein show equal efficiency in protection from complement-mediated cell damage, J. Exp. Med. 174 (1991) 35–44.

[12] F. Santoro, P.E. Kennedy, G. Locatelli, M.S. Malnati, E.A. Berger, P. Lusso, CD46 is a cellular receptor for human herpesvirus 6, Cell 99 (1999) 817–827.

[13] R.E. Dorig, A. Marcil, A. Chopra, C.D. Richardson, The human CD46 molecule is a receptor for measles virus (Edmonston strain), Cell 75 (1993) 295–305.

[14] H. Kallstrom, M.K. Liszewski, J.P. Atkinson, A.B. Jonsson, Membrane cofactor protein (MCP or CD46) is a cellular pilus receptor for pathogenic *Neisseria*, Mol. Microbiol. 25 (1997) 639–647.

[15] N. Okada, M.K. Liszewski, J.P. Atkinson, M. Caparon, Membrane cofactor protein (CD46) is a keratinocyte receptor for the M protein of the group A streptococcus, Proc. Natl. Acad. Sci. U. S. A. 92 (1995) 2489–2493.

[16] K. Iwata, T. Seya, Y. Yanagi, J.M. Pesando, P.M. Johnson, M. Okabe, S. Ueda, H. Ariga, S. Nagasawa, Diversity of sites for measles virus binding and for inactivation of complement C3b and C4b on membrane cofactor protein CD46, J. Biol. Chem. 270 (1995) 15148–15152.

[17] M. Manchester, A. Valsamakis, R. Kaufman, M.K. Liszewski, J. Alvarez, J.P. Atkinson, D.M. Lublin, M.B. Oldstone, Measles virus and C3 binding sites are distinct on membrane cofactor protein (CD46), Proc. Natl. Acad. Sci. U. S. A. 92 (1995) 2303–2307.

[18] H.L. Greenstone, F. Santoro, P. Lusso, E.A. Berger, Human herpesvirus 6 and measles virus employ distinct CD46 domains for receptor function, J. Biol. Chem. 277 (2002) 39112–39118.

[19] T. Seya, M. Kurita, K. Iwata, Y. Yanagi, K. Tanaka, K. Shida, M. Hatanaka, M. Matsumoto, S. Jun, A. Hirano, S. Ueda, S. Nagasawa, The CD46 transmembrane domain is required for efficient formation of measles-virus-mediated syncytium, Biochem. J. 322 (Pt 1) (1997) 135–144.

[20] T. Seya, T. Hara, M. Matsumoto, H. Akedo, Quantitative analysis of membrane cofactor protein (MCP) of complement. High expression of MCP on human leukemia cell lines, which is down-regulated during cell differentiation, J. Immunol. 145 (1990) 238–245.

[21] F. Sakurai, K. Kawabata, T. Yamaguchi, T. Hayakawa, H. Mizuguchi, Optimization of adenovirus serotype 35 vectors for efficient transduction in human hematopoietic progenitors: comparison of promoter activities, Gene Ther. 12 (2005) 1424–1433.